

# Manufacturing synthetic viscoelastic antigen-presenting cells for immunotherapy

Zeyang Liu<sup>1,6</sup>, Yan-Ruide Li<sup>1,2,6</sup>, Youcheng Yang<sup>1,6</sup>, Enbo Zhu<sup>1</sup>, Haochen Nan<sup>1</sup>, Yue Yan<sup>1</sup>, Bo Zhang<sup>1</sup>, Guorui Chen<sup>1</sup>, Nicolas Pedroncelli<sup>1</sup>, Zibai Lyu<sup>1,2</sup>, Jason Lin<sup>1</sup>, Jennifer Soto<sup>1</sup>, Lili Yang<sup>1,2,3,4,5</sup>✉ & Song Li<sup>1,3,4</sup>✉

## Abstract

This protocol details the preparation and functionalization of viscoelastic synthetic antigen-presenting cells (APCs) for T cell activation, designed to enhance immunotherapeutic efficacy. Using a high-throughput microfluidic system and post-processing, we create cell-sized sodium alginate microbeads with tunable stiffness, viscoelasticity and surface chemistry, enabling them to better mimic the physical and activation properties of natural APCs. The protocol includes fabrication of synthetic cells with defined sizes, crosslinking strategies to achieve desirable mechanical properties, surface functionalization via click chemistry for attaching activation molecules, and characterization methods for mechanical and biochemical properties. Compared with traditional matrices or rigid microbeads, this approach allows precise control over the mechanical and biochemical features of synthetic APCs, ensuring optimal T cell activation. The resulting synthetic cells support robust T cell activation and expansion, enhance the CD8/CD4 T cell ratio, promote T memory stem cell (TMSC) formation and improve chimeric antigen receptor transduction efficiency, leading to superior tumor-killing efficacy in vitro and in vivo. Additionally, these synthetic cells can be efficiently removed from T cells after activation using simple centrifugation or calcium chelation, preserving the activated T cells. The complete protocol, including fabrication, functionalization and quality assessment, requires ~1 week to complete. Users should have experience in microfluidics, biomaterial handling, bioconjugation techniques and basic cell culture. This platform can be adapted for broader applications in immune cell engineering.

## Key points

- Protocol describing the fabrication of synthetic viscoelastic antigen-presenting cells and their application in T cell engineering, including crosslinking strategies to achieve desirable mechanical properties, surface functionalization via click chemistry for attaching activation molecules, and characterization methods for mechanical and biochemical properties.
- These synthetic cells support robust T cell expansion, which contributes to longer in vivo persistence, stronger antitumor immune responses and improved tumor control than those expanded with conventional methods.

## Key reference

Liu, Z. et al. *Nat. Biomed. Eng.* **8**, 1615–1633 (2024): <https://doi.org/10.1038/s41551-024-01272-w>

<sup>1</sup>Department of Bioengineering, University of California Los Angeles, Los Angeles, CA, USA. <sup>2</sup>Department of Microbiology, Immunology and Molecular Genetics, University of California, Los Angeles, Los Angeles, CA, USA. <sup>3</sup>Eli and Edythe Broad Centre of Regenerative Medicine and Stem Cell Research, University of California, Los Angeles, Los Angeles, CA, USA. <sup>4</sup>Jonsson Comprehensive Cancer Centre, University of California, Los Angeles, Los Angeles, CA, USA. <sup>5</sup>Molecular Biology Institute, University of California, Los Angeles, Los Angeles, CA, USA. <sup>6</sup>These authors contributed equally: Zeyang Liu, Yan-Ruide Li, Youcheng Yang. ✉e-mail: [liliyang@ucla.edu](mailto:liliyang@ucla.edu); [songli@ucla.edu](mailto:songli@ucla.edu)

## Introduction

In recent years, chimeric antigen receptor-engineered T cell (CAR-T) therapy has garnered attention for its remarkable efficacy in treating hematologic malignancies<sup>1–4</sup>. This innovative therapy broadly involves isolating a patient's T cells, genetically modifying them to target specific cancer antigens and reintroducing them into the body to induce a targeted immune response. While CAR-T therapy has shown remarkable success in treating certain blood cancers, its effectiveness is constrained by variability in expanded cell populations, suboptimal T cell subtypes following ex vivo expansion and limited therapeutic efficacy in solid tumors<sup>5–8</sup>. During the ex vivo expansion of CAR-T cells, conventional activation methods—such as using anti-CD3/anti-CD28 antibody-coated paramagnetic beads (for example, Dynabeads)—lack the physiological levels of mechanical and biochemical cues that are essential for optimal T cell activation, differentiation and sustained efficacy<sup>9–24</sup>. As a result, CAR-T cells activated through these rigid beads often exhibit reduced stemness and persistence, thus limiting their overall therapeutic efficacy<sup>25</sup>.

Natural antigen-presenting cells (APCs) provide dynamic mechanical presentation of activation signals through their distinct viscoelasticity, which has a crucial role in T cell activation, proliferation and differentiation. Studies suggest activation platforms that better emulate the flexible, viscoelastic nature of natural cells can enhance T cell stemness and improve long-term tumor control<sup>26,27</sup>. This unmet need for a more biomimetic T cell activation highlights the importance of advancing CAR-T manufacturing technology and optimizing it for broader applications in immunotherapy.

To address these limitations, we have developed a novel biomaterial platform termed synthetic viscoelastic T cell-activating cells (synthetic cells)<sup>27</sup>. Synthetic cells are micro-sized spheres engineered to closely recapitulate the mechanical characteristics of natural APCs, including key tunable features such as viscoelasticity and stiffness (Fig. 1). Unlike traditional elastic or rigid microspheres, the viscoelastic properties of synthetic cells provide physiologically relevant, dynamic mechanical signals that are crucial for maintaining T cell stemness, enhancing CAR transduction efficiency and promoting robust and durable antitumor activity.

This protocol describes the preparation and functionalization of synthetic cells for the activation and expansion of T cells, detailing each step of the fabrication process, functionalization and quality control measures to ensure reproducibility and consistency. By offering a method that better mimics the natural biophysical properties T cell activation environment, this protocol aims to improve the quality and therapeutic potential of CAR-T cells, with broad applications in cancer immunotherapy and beyond.

## Development of the protocol

The development of synthetic cells was motivated by the need for a biomimetic platform that could enhance T cell activation and expansion by providing both biochemical and mechanical cues that closely resemble those of natural APCs<sup>27</sup>. Our initial studies focused on designing and fabricating synthetic cells using a microfluidic system, allowing for high-throughput production with precise control over cell size and mechanical properties. By optimizing factors such as alginate formulation and crosslinker concentration, we achieved a system that effectively mimics the viscoelastic and elastic characteristics of natural APCs (Fig. 2). These characteristics include a finely tuned stiffness and relaxation time, which are essential for presenting the activation signals on the surface of the microbeads and creating a dynamic interaction with T cells.

Our research demonstrates that tuning the stiffness and viscoelastic properties of synthetic cells influences T cell activation. The generated microbeads can be modified with click chemistry to present activation signals such as antibodies and antigens<sup>27</sup>. Assuming linear extrapolation during scale-up production, we estimate that 10 parallel microfluidic chips can generate  $6 \times 10^8$  synthetic cells within 24 h. These can be used to activate and expand  $\sim 10^{10}$ – $10^{11}$  CAR-T cells, which can be formulated into  $\sim 100$ – $1,000$  doses ( $\sim 10^8$ – $10^9$  cells per dose, based on approved CAR-T cell therapy doses<sup>27,28</sup>).

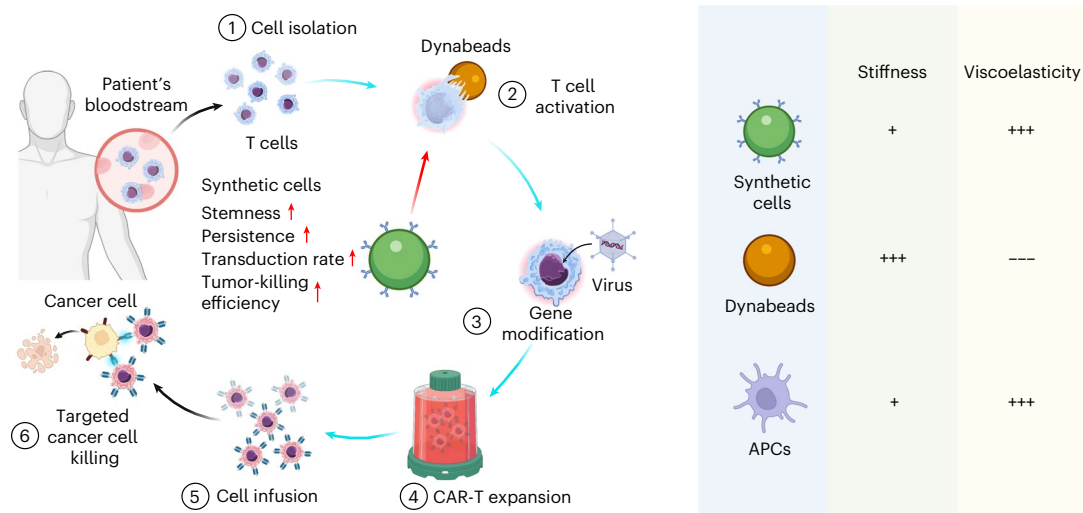


**Fig. 1 | Workflow of CAR T cell generation and the role of synthetic viscoelastic APCs (synthetic cells) in enhancing cancer immunotherapy.** The process begins with T cell isolation from the patient's bloodstream (1). The isolated T cells can be activated using either synthetic cells or Dynabeads during T cell activation (2). Synthetic cells enhance T cell stemness, persistence, transfection efficiency and tumor-killing capabilities compared with Dynabeads. Following activation, the T cells undergo gene modification via viral transduction to introduce a chimeric antigen receptor (CAR) (3), followed by CAR expression

and CAR T cell expansion (4) and T cell infusion (5). The resulting CAR T cells are then used in targeted cancer cell killing, where they specifically identify and kill cancer cells (6). Right: the differences in stiffness and viscoelasticity among synthetic cells, Dynabeads and APCs. Synthetic cells closely mimic the physical properties of natural APCs, with moderate stiffness and enhanced viscoelasticity, making them particularly effective in promoting T cell functionality. The '+' and '-' symbols indicate positive or negative effects, with the number of symbols reflecting relative magnitude.

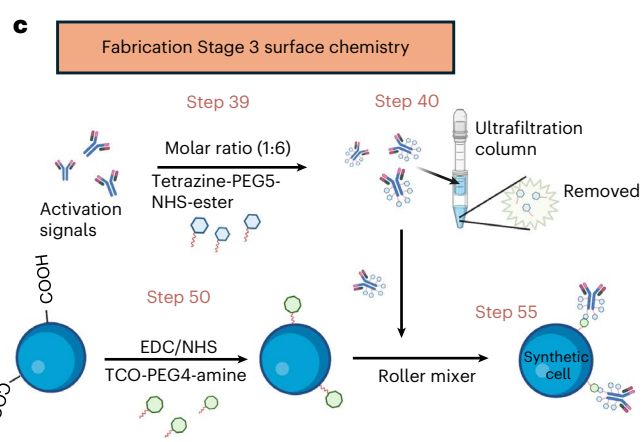
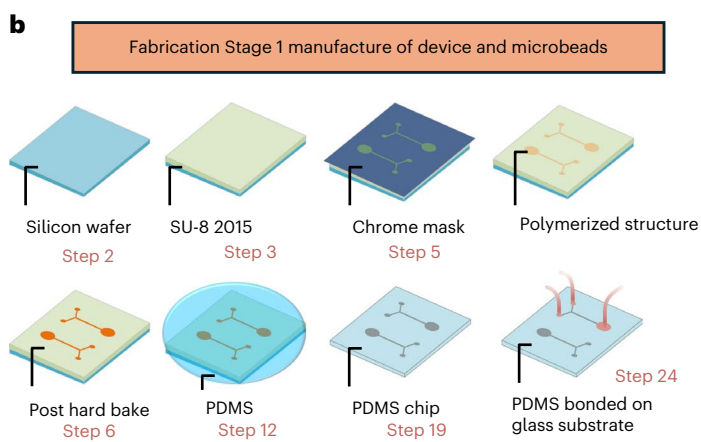
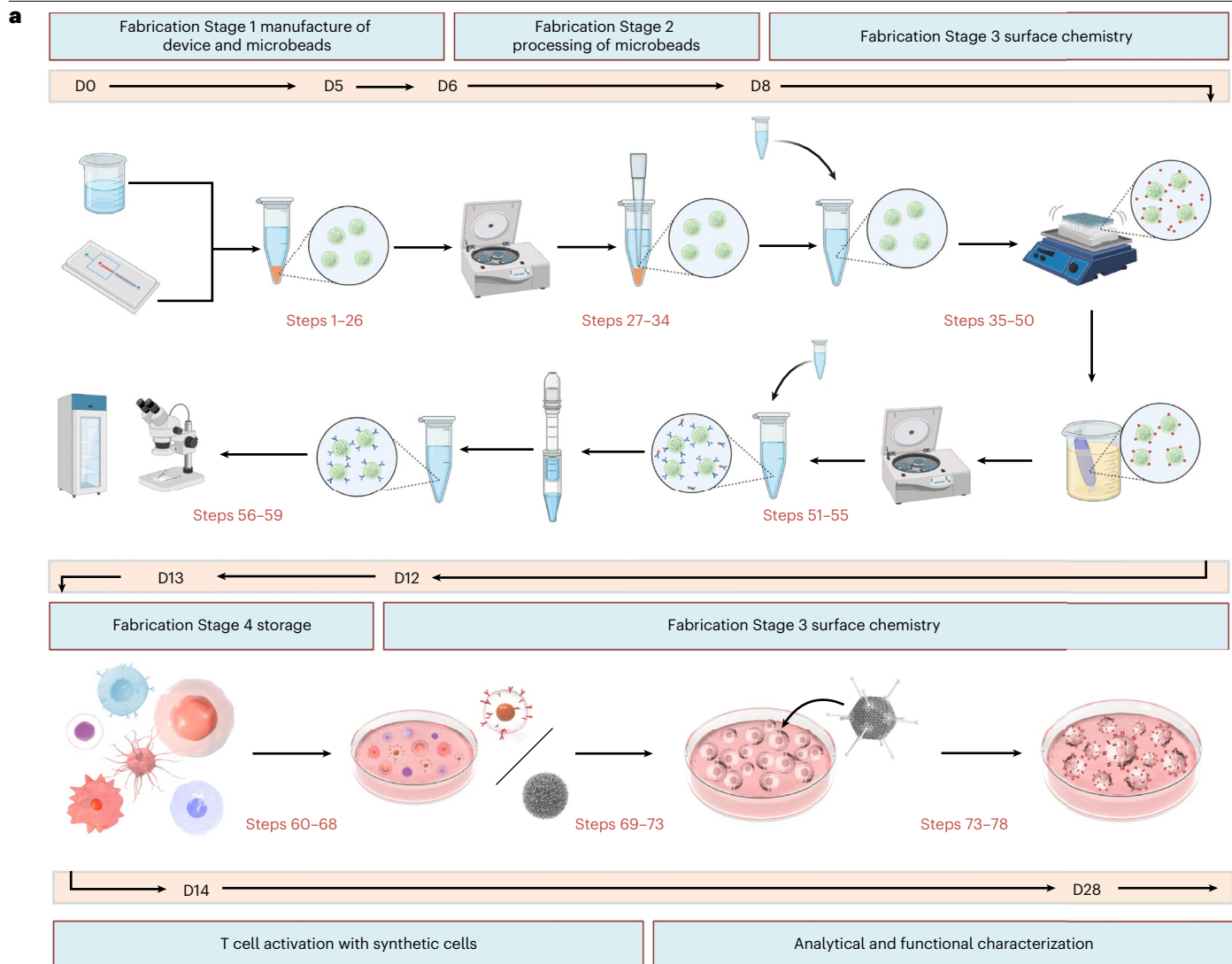
In addition, these microbeads can be separated from T cells by simple centrifugation and the change of cell culture medium, or viscoelastic microbeads can also be dissolved by adding a calcium chelator such as ethylenediaminetetraacetic acid (EDTA) to disrupt the ionic crosslinking of alginate polymer. EDTA treatment rapidly dissolves all synthetic cells, thereby minimizing physical disruption and potential impacts on the immunological synapse. In addition, the synthetic cell product can be stored under refrigerated conditions (4 °C) for at least 60 d. For longer-term storage, synthetic cells can be preserved at -20 °C in a storage buffer containing trace amounts of calcium ions and an appropriate concentration of glycerol to maintain stability. Further research is required to establish optimal storage conditions for maximizing their longevity and functionality.

These advantages make the method suitable for future clinical and commercial development. In head-to-head comparisons with conventional activators such as Dynabeads, synthetic cells promoted a higher percentage of CD8<sup>+</sup> T cells and TMSCs and showed improved CAR transduction efficiency and tumor cell-killing capabilities<sup>27</sup>. Furthermore, our findings underscore the critical role of viscoelasticity in enhancing CAR-T cell functionality and persistence in vivo. This protocol was developed to guide researchers in replicating this innovative platform, enabling a more physiologically relevant approach to T cell engineering and immunotherapy.

## Overview of the procedure

This protocol describes the fabrication of our synthetic cell, which comprises four fabrication stages (Fig. 2). Fabrication Stage 1 of the procedure describes the manufacture of the microfluidic device and its use in the production of uniform alginate-based microbeads (Steps 1–26). Fabrication Stage 2 describes the purification of the microbeads and optional crosslinking to adjust mechanical properties (Steps 27–34). Fabrication stage 3 describes surface functionalization via click chemistry (Steps 35–55). Fabrication Stage 4 describes the steps required to store microbeads (Steps 56–59). We also detail the follow-up steps required for T cell activation with synthetic cells (Steps 60–77), and a range of downstream assays to characterize the synthetic cells.

# Protocol



Our Procedure details four distinct formulations for synthetic cells that, together, span a wide range of mechanical properties, tailored to closely mimic the viscoelastic characteristics of natural APCs. These formulations and methods are provided as guidelines and can be further

**Fig. 2 | Workflow for the preparation and application of synthetic cells in T cell activation and functional characterization.** **a**, The workflow consists of four main fabrication stages. Stage 1: manufacture of device for fabricating synthetic cells (Steps 1–26) using microfluidic systems; Stage 2: processing of microbeads (Steps 27–34) to remove impurities and manipulate the mechanical properties; Stage 3: surface chemistry (Steps 35–55) for surface functionalization through chemical modification; and Stage 4: storage (Steps 56–59) for handling

and preserving purified synthetic cells. The follow-up steps (Steps 60–78) involve T cell activation and analytical and functional characterization to evaluate their effectiveness in enhancing T cell responses. **b**, The detailed microfabrication process in fabrication Stage 1: manufacture of device and microbeads. **c**, The detailed surface modification process in fabrication Stage 3: surface chemistry. D0–D28, days 0–28.

optimized to meet specific experimental needs. The following sections outline key parameters to consider when adapting this protocol, including cell size, ligand density and mechanical tuning, to achieve optimal T cell activation and functionality.

## Applications

Synthetic cells are an advanced platform to improve the activation, expansion and functionality of T cells for cancer immunotherapy, with a particular focus on enhancing the therapeutic potential of CAR-T cells. Unlike traditional T cell activators, synthetic cells simulate the mechanical cues present in natural APCs, providing a more physiologically relevant environment that supports long-term T cell functionality and persistence. This innovative approach has notable implications for treating a variety of cancers, especially in cases where existing CAR-T therapies have shown limitations in durability and efficacy.

One of the most promising applications of synthetic cells lies in their ability to enhance the generation of TMSCs. TMSCs have the unique ability to self-renew and differentiate into various T cell subsets, which are essential for sustained antitumor immunity<sup>29,30</sup>. In our previous studies, T cells expanded using synthetic cells exhibited not only a higher proportion of TMSCs compared with those activated with conventional methods such as Dynabeads, but also an increased population of CD8<sup>+</sup> cytotoxic T cells and a reduction in regulatory T (T<sub>reg</sub>) cells<sup>27</sup>. These combined effects contribute to longer in vivo persistence, stronger antitumor immune responses and improved tumor control. Additionally, synthetic cells have been shown to increase CAR-T cell transduction efficiency, resulting in a greater number of CAR-expressing T cells with robust antitumor activity<sup>27</sup>. In preclinical models, CAR-T cells activated with synthetic cells demonstrated superior tumor-killing capacity against solid tumors and hematologic malignancies in mouse models. This improved functionality is particularly valuable for targeting solid tumors, where CAR-T cells must overcome an immunosuppressive tumor microenvironment. The viscoelastic properties of synthetic cells support a dynamic interaction with T cells, enabling sustained activation and enhanced cytotoxic potential in these challenging environments.

Furthermore, although not yet experimentally demonstrated, synthetic cells potentially offer adaptability for a wide range of immunotherapeutic applications beyond CAR-T cell therapies. By customizing the surface chemistry and mechanical properties, synthetic cells can be used to activate and expand other immune cell types, such as natural killer cells or tumor-infiltrating lymphocytes, which are being explored as promising therapies for various cancers. This versatility makes synthetic cells a valuable tool in the broader field of cancer immunotherapy, with the potential to enhance immune cell-based treatments across multiple cancer types.

## Comparison with other methods

T cell activation is a critical process in the immune response, where T cells recognize peptide–MHC complexes presented by APCs through their T cell receptors (TCRs)<sup>7</sup>. The immune synapse, a specialized junction formed between the T cell and APC, has a vital structural and functional role in this process, organizing signaling molecules, adhesion proteins and cytoskeletal elements to ensure effective activation<sup>31,32</sup>. This dynamic interaction allows for the precise coordination of antigen recognition, costimulation and cytolytic granule or cytokine release toward a polarized target<sup>31,33</sup>. To replicate these complex interactions in vitro and induce T cell activation and expansion ex vivo, several strategies have been developed (Table 1). Historical approaches include a T cell coculture with cellular-based APCs, such as

**Table 1 | Summary of mechanical properties and characteristics of synthetic APC products for polyclonal human T cell activation and expansion**

Cell products	Mechanical property		Size/geometry	Other benefits	Refs.
	Stiffness	Viscoelasticity <sup>a</sup>			
Synthetic cells	Low (10–30 kPa)	High (10–100 s)	Tunable (7–10 μm)	High degree of tunability toward native APC characteristics	27
Pulsed APCs	Low (0.1–20 kPa)	High (10–100 s)	5–12 μm	Natural APCs	37–39
Spherical magnetic microparticles (Dynabeads)	High (1–4 GPa)	N/A	1–5 μm	–	40,46
Polymeric nanomatrix (TransAct)	Unknown	Unknown	~50–500 nm	Simple separation	45,48
Mesoporous silica rods with supported lipid bilayers	Unknown; combination of silica microrods and liposomes	Unknown; non-zero due to membrane fluidity	~70 μm × ~5 μm microrods; curved lipid bilayer	Gradual release of soluble, mitogenic cues	9
Cell-sized lipid vesicles	Unknown	High membrane fluidity	20 μm	Can use relatively low APC-to-T cell ratio (1:17)	84
Alginate-based artificial antigen presenting cells	Unknown	Unknown; non-zero due to ionic crosslink	500–600 nm	Expand functional CD8 <sup>+</sup> T cells with memory characteristics	85
Cell-templated silica microparticles with supported lipid bilayers	Unknown	Unknown; non-zero due to membrane fluidity	Red blood cell: 4.5 μm Microsphere: 8 μm HeLa: 16 μm	Promote CD8 <sup>+</sup> T cell growth over CD4 <sup>+</sup> T cell growth	86
Surface-functionalized microgels	Low (1–5 kPa)	Unknown	20–80 μm	Layer-by-layer coating using oppositely charged polymers	87
Thiolated hyaluronic acid reacted with PEG-diacrylate and antibodies	Low (0.5–3 kPa)	N/A	Large polymer network	T cell (CD44) engagement with HA	88
PLGA spherical particles with surface cue-tethered to DNA attached to polymer via 5k-PEG linkers	High (1–4 GPa)	Unknown; dynamic flexibility of DNA linker	1–2 μm; spherical nanoparticle	Surface presentation of a cytokine (IL-2)	89
Semiflexible polyisocyanopeptide polymer-based immunobrushes	Unknown	Unknown	3D-brush network on surface of magnetic beads	Dynamic fluidity from polymer brush behavior	90

<sup>a</sup>Viscoelasticity is represented using the 50% stress relaxation time, where a smaller value indicates stronger viscoelasticity.

autologous, patient-derived APCs, monocyte-derived dendritic cells (moDCs) or genetically engineered stable cell lines, to closely mimic the immune interactions in the body<sup>34–38</sup>. While these methods reproduce the dynamic and mechanical properties of the natural immune synapse, they are limited by the labor-intensive processes associated with cell isolation and culture; the expression levels of TCRs and costimulatory ligands, which are prone to genetic drift, are also difficult to control in these cell lines, emphasizing the need for the development of reproducible, artificial-APCs for stimulating T cell activation<sup>34,35,39</sup>.

Artificial APC strategies typically involve the immobilization of anti-CD3/anti-CD28 antibodies onto various materials, such as culture plate surfaces, rigid microbeads or polymer networks, to cluster the TCR signaling machinery and provide costimulation in a controllable and simplified model of the immune synapse (Table 1). Several strategies have revealed the effects of various artificial APC biophysical parameters on T cell activation, such as APC stiffness, membrane geometry and antigen fluidity, which refers to the lateral mobility of antigen-presenting molecules on the APC surface, influencing TCR clustering and activation efficiency<sup>40–43</sup>. However, while these platforms can robustly activate T cells, they have yet to be optimized to replicate the dynamic synapse interactions provided by natural APCs, such as cellular deformation, membrane partitioning or time-dependent biomechanical signals, which may be essential for optimal T cell activation and differentiation. To address these limitations, we developed synthetic cells, composed of cell-sized sodium alginate microbeads with tuneable stiffnesses and viscoelasticity to better recapitulate the deformable characteristics of APCs in vivo. We hypothesized that the necessary dynamic interactions within the activating T cell synapse can be elicited particularly by material viscoelasticity, which has been shown to be

a driving force behind T cell phenotype differentiation but not investigated in artificial APC platforms to our knowledge.

Here, we specifically compare the performance and limitations of synthetic cells against clinically translated platforms, such as Dynabeads and TransAct<sup>44,45</sup>. Dynabeads are superparamagnetic polystyrene beads, widely used for T cell activation and expansion owing to their ability to present anti-CD3/anti-CD28 antibodies, which are essential for TCR engagement and costimulation<sup>46</sup>. However, Dynabeads are rigid, lacking the mechanical flexibility and viscoelastic properties that are characteristic of natural APCs<sup>46</sup>. This rigidity limits their ability to support optimal T cell activation, stemness and persistence. Studies show that T cells activated by Dynabeads tend to exhibit lower levels of TMSCs and may experience rapid differentiation, reducing their long-term therapeutic efficacy<sup>47</sup>. TransAct, a T cell activator composed of a proprietary polymeric nanomatrix coated with anti-CD3/anti-CD28 antibodies, presents an alternative approach by enabling polyclonal T cell activation without the use of solid beads. Although TransAct provides the necessary biochemical signals for T cell activation, it probably lacks the physical scaffold and geometry required for optimal mechanical feedback during immune synapse formation<sup>45,48</sup>. This absence of mechanical engagement can lead to suboptimal T cell expansion and functional outcomes as T cells activated in suspension may not achieve the same level of activation as those interacting with a surface. In contrast, our newly developed synthetic cells overcome the limitations of Dynabeads and TransAct by combining biochemical signals with a solid (yet tuneable and flexible) structure, mimicking the interaction dynamics of T cells with natural APCs and enabling more robust activation. Their biomimetic design thus offers a new cell therapy manufacturing strategy, enhancing CAR-T cell transduction efficiency and supporting the formation of TMSCs, which are crucial for the long-term persistence, therapeutic durability and antitumor functionality not seen with traditional methods.

Additionally, synthetic cells provide customization and adaptability as they can be tailored for various immune cell applications by adjusting parameters such as ligand density, mechanical stiffness and surface functionalization. This flexibility allows synthetic cells to support a broad spectrum of immunotherapy applications, including the activation of natural killer cells, tumor-infiltrating lymphocytes and other immune cell types. By integrating both biochemical signals and dynamic mechanical properties, synthetic cells offer a more sophisticated and versatile alternative to existing T cell activators, presenting a promising tool for advancing CAR-T cell therapies and other immune cell-based treatments.

A distinctive advantage of synthetic cells over both Dynabeads and TransAct is their capability for antigen-specific activation. By conjugating specific antigens, such as mesothelin, to synthetic cells, we can achieve highly targeted T cell activation. In our previous studies, mesothelin-conjugated synthetic cells demonstrated superior specificity and activation strength compared with pulsed mDCs, a conventional method for antigen-specific activation<sup>27</sup>. This specificity is not only more efficient but also scalable, making it adaptable for a wider range of applications, including TCR-based therapies. By enabling controlled and specific T cell activation, synthetic cells open the door for personalized immunotherapy approaches that can target distinct cancer antigens. The flexibility of this system also allows researchers to customize synthetic cells for different antigens or costimulatory ligands, supporting precise T cell expansion protocols that are essential for TCR and other antigen-specific therapies.

## Limitations

The fabrication of synthetic cells requires a multidisciplinary skill set, including expertise in microfluidics, micro-nanofabrication and organic chemistry. One of the primary challenges is the need for a microfluidic chip fabrication platform, typically accessible only at larger research institutions owing to the high costs associated with materials, equipment and specialized training<sup>49–52</sup>. Micro-nanofabrication is a highly skilled process; although this protocol provides comprehensive engineering design files, the accuracy of mask fabrication is not only determined by the precision of the photolithography equipment but also heavily reliant on the operator's proficiency<sup>53–57</sup>. Variations in fabrication expertise can lead to slight differences in microchannel dimensions within the microfluidic device, which in turn affects flow rates and could introduce variability in synthetic cell production.

To ensure reproducibility, high-resolution masks are essential for microfluidic chip fabrication. For instance, critical dimension specifications from the UCLA Mask Shop indicate a resolution of 3  $\mu\text{m}$  with a tolerance of  $\pm 0.2 \mu\text{m}$ . This tolerance is set based on the resolution limits of standard photolithography processes and ensures that microfluidic channel dimensions remain within acceptable variation ranges for stable fluid dynamics and reproducible synthetic cell production. While the critical dimension can be pushed to 2  $\mu\text{m}$ , the final precision strongly depends on the layout and is not always guaranteed. Our experience with different mask types has shown that chrome masks consistently achieve the required precision, whereas file masks often exceed a 1  $\mu\text{m}$  tolerance in fine structural regions, leading to potential deviations in microchannel dimensions. These dimensional variations can affect flow rates and introduce variability in synthetic cell production. Thus, careful consideration of mask fabrication methods is necessary to maintain reproducibility. Researchers without direct access to photolithography facilities may need to collaborate with specialized microfabrication services to ensure optimal mask quality and device performance.

Additionally, the successful functionalization of synthetic cells through click chemistry requires foundational knowledge of organic chemistry. Although detailed reagent proportions are provided in this protocol, adjustments may be necessary depending on specific experimental conditions, equipment and container materials. Furthermore, the current protocol employs NHS-ester chemistry in both the covalent crosslinking step (for generating elastic microbeads via adipic acid dihydrazide (AAD)) and the surface conjugation step (for example, TCO-PEG4-amine modification), which use carboxyl groups on alginate. Although carboxyl group availability was not a limiting factor under our experimental conditions, future iterations of the protocol could benefit from incorporating orthogonal chemistries, such as those involving oxidized hydroxyl groups. These alternative strategies may enhance modularity and minimize crossreactivity between internal crosslinking and surface modification steps. However, implementing such approaches often relies on empirical optimization, which may present challenges for laboratories lacking extensive expertise in organic synthesis. These limitations underscore the technical challenges and inherent variability in synthetic cell production, highlighting the need for continued research and refinement to improve accessibility and reproducibility.

## Expertise needed to implement the protocol

Implementing this protocol requires a foundational knowledge of cell culture techniques and biomaterial handling, as well as specific skills in microfluidic systems, including the operation of droplet-based or flow-focusing microfluidic devices, pressure control systems and microfabrication techniques for the fabrication of synthetic cells. If researchers are unfamiliar with these techniques, prefabricated microfluidic chips can be obtained from commercial suppliers or university core facilities. To broaden accessibility, alternative methods beyond microfluidic-based fabrication can be considered for producing synthetic cells. Bulk emulsions using a homogenizer or other nonmicrofluidic droplet generation techniques have been widely used to create microbeads below 10  $\mu\text{m}$  in diameter<sup>58–60</sup>. However, a key limitation of these methods is that the size distribution of the resulting microbeads is generally broader, making it difficult to achieve the same level of uniformity as microfluidic-based approaches. As bead size can influence physical interactions with T cells, maintaining a controlled size range is advantageous in ensuring reproducibility.

Researchers should also be familiar with handling primary T cells, including isolation and culture, as well as flow cytometry for assessing T cell activation, expansion and phenotype. For surface chemistry functionalization, experience with bioconjugation techniques, such as click chemistry or carbodiimide crosslinking, is recommended to optimize ligand attachment on synthetic cells for both polyclonal and antigen-specific activation. Basic laboratory safety and aseptic techniques are essential, especially for those working with live cells and potentially immunogenic materials. As this protocol is designed to be accessible to experienced researchers, those without expertise in microfluidic systems or surface chemistry may benefit from collaborating with specialists or utilizing contract research services for device fabrication and ligand conjugation.

**Table 2 | Different formulations of synthetic cell production**

Synthetic cells/elastic beads formulation	Stiffness <i>E</i> (kPa)	Stress relaxation time $t_{1/2}$ (s)	Antibodies/bead	Size ( $\mu\text{m}$ )
V1 (soft viscoelasticity)	15	10	$10^{5.9}$	~7–9
V2 (stiff viscoelasticity)	25	10	$10^{5.9}$	~7–9
E1 (soft elastic)	15	1,500	$10^{5.9}$	~7–9
E2 (stiff elastic)	25	1,500	$10^{5.9}$	~7–9

## Experimental design

### Tuning mechanical properties

The viscoelasticity and stiffness of synthetic cells are crucial for mimicking natural APCs. By adjusting crosslinking and polymer composition, this protocol enables tuning of the mechanical properties across a wide range, facilitating T cell activation that more closely resembles physiological conditions. In this protocol, we specify formulations V1 (soft viscoelastic) and V2 (stiff viscoelastic) microbeads, as well as E1 (soft elastic) and E2 (stiff elastic) microbeads (Tables 2 and 3). While viscoelastic formulations (V1 and V2) are designed to mimic the dynamic mechanical behavior of natural APCs, the elastic formulations (E1 and E2) serve as important controls to isolate the effects of stiffness alone, independent of stress relaxation. These formulations are particularly useful for researchers aiming to dissect the distinct roles of stiffness versus viscoelasticity in modulating T cell activation and phenotype, a topic of interest in immune cell mechanobiology.

It is important to remember that viscoelasticity refers to the time-dependent mechanical response of a material, exhibiting both elastic (solid-like) and viscous (fluid-like) properties when subjected to stress or deformation. Unlike purely elastic materials, viscoelastic materials display stress relaxation, meaning they gradually dissipate stress under a constant strain over time<sup>61,62</sup>. This behavior is essential in biological tissues and biomaterials as it influences how cells sense and respond to their mechanical microenvironment. Therefore, selecting the right mechanical profile is essential for specific applications, such as promoting TMSC formation. As an example, the biomaterial-based synthetic cells possess mechanical properties that closely mimic native APCs, particularly immature dendritic cells, which typically have a size of 6–9  $\mu\text{m}$ , a stiffness range of 1–11 kPa and a half-stress relaxation time of 1–5 s (ref. 63). By tuning the stiffness and viscoelasticity of synthetic cells within this range, we aimed to replicate the dynamic biophysical cues provided by natural APCs, thereby optimizing T cell activation and differentiation. Indeed, other examples highlight the importance of mechanical tuning in immune cell engineering, such as with the role of mechanical stiffness in Notch signaling. Studies have shown that DLL4-mediated Notch activation in hematopoietic stem cells can be enhanced using more rigid surfaces (stiffness >30 kPa), which promote T cell differentiation<sup>64,65</sup>. In contrast, softer substrates may better preserve hematopoietic stem cell stemness<sup>66,67</sup>. Here, different stiffness ranges could potentially be leveraged to guide specific cell fate decisions.

The stiffness of synthetic cells is a key parameter influencing T cell activation and phenotype. In this protocol, stiffness is tuned through two main strategies. For viscoelastic formulations (V1 and V2), stiffness is primarily controlled by adjusting the ionic crosslinking strength, specifically by varying the concentration of  $\text{Ca}^{2+}$  in the EDTA- $\text{Ca}^{2+}$

**Table 3 | Material components used in synthetic cell assembly**

Synthetic cells formulation (per 3M batch)	Alginate		HFE-7500 used	EDC/NHS used	HoBt/AAD used	TCO/Tetrazine used	Antibody used
	Mass	Average molecular weight					
E1 (soft elastic)	0.2 mg	120 kDa	50 $\mu\text{L}$	84/18 mg	4.2/1.248 mg	2 $\mu\text{mol}$ /135 pmol	6 $\mu\text{g}$
E2 (stiff elastic)	0.2 mg	120 kDa	50 $\mu\text{L}$	84/18 mg	12/6.24 mg	2 $\mu\text{mol}$ /135 pmol	6 $\mu\text{g}$
V1 (soft viscoelasticity)	0.2 mg	75 kDa	50 $\mu\text{L}$	24/18 mg	0/0 mg	2 $\mu\text{mol}$ /135 pmol	6 $\mu\text{g}$
V2 (stiff viscoelasticity)	0.2 mg	75 kDa	50 $\mu\text{L}$	24/18 mg	0/0 mg	2 $\mu\text{mol}$ /135 pmol	6 $\mu\text{g}$

buffer during bead fabrication (Tables 2 and 3). For elastic formulations, stiffness is tuned during a secondary covalent crosslinking step. Specifically, the concentration of 1-ethyl-3-(3-dimethylaminopropyl)carbodiimide (EDC) is kept in excess to initiate crosslinking, while the levels of 1-hydroxybenzotriazole (HoBt) and AAD are varied to control the degree of crosslinking. Higher concentrations of HoBt and AAD yield stiffer microbeads (for example, E2), while lower concentrations produce softer beads (for example, E1). If needed, these concentrations can be further adjusted to fine-tune stiffness for specific experimental goals.

## Controlling size

Synthetic cells are fabricated in different size ranges to optimize T cell engagement. Size influences the cell's interaction surface and signal presentation, affecting TCR clustering and activation. This protocol allows for fine-tuning of synthetic cell size based on intended applications, typically between 5 and 10  $\mu\text{m}$ . Size plays a critical role in T cell activation efficiency. From a biomimetic perspective, beads in the range of 5–15  $\mu\text{m}$  are considered optimal, as they can facilitate immunological synapse formation, mimicking the natural interactions between T cells and APCs. However, the impact of bead size on T cell activation is complex and may also be influenced by ligand density and surface receptor interactions. It has been hypothesized that bead size-mediated CD45 exclusion from TCR–ligand contacts shifts the immunoreceptor tyrosine-based activation motif (ITAM) phosphorylation–dephosphorylation balance, thereby influencing TCR signaling<sup>68</sup>. Specifically, smaller beads may promote CD45 exclusion, enhancing TCR activation by reducing phosphatase-mediated inhibition. However, this hypothesis has not been systematically validated, and the precise relationship between bead size, ligand presentation and T cell activation efficiency requires further investigation.

## Scale

This protocol supports scalable production using a high-throughput microfluidic system, making it suitable for both research and translational settings. Production scalability allows for consistent fabrication of synthetic cells in large quantities while maintaining controlled properties across batches.

## TCR and costimulatory ligands

Surface conjugation of TCR and costimulatory ligands (for example, anti-CD3/anti-CD28) is essential for effective T cell activation<sup>69–73</sup>. This protocol allows for precise control over ligand density, supporting both polyclonal and antigen-specific activation, thereby expanding the range of possible applications in CAR-T and TCR therapies. The selection of anti-CD3 and anti-CD28 antibodies remains the standard approach for polyclonal T cell activation, as it provides both signal 1 (TCR activation) and signal 2 (costimulation). Our synthetic cell system is designed to maintain a 1:1 anti-CD3: anti-CD28 ratio, ensuring consistent ligand presentation. However, further optimization of ligand density and ratios could enhance T cell activation efficiency. Studies suggest that ligand organization and density on artificial APCs influence TCR clustering and downstream signaling, making this an important consideration for future design improvements<sup>74</sup>. Moreover, enhancing immunological synapse formation through additional ligands could be a promising future direction. For instance, incorporating intercellular adhesion molecule 1 (ICAM-1) could strengthen cell adhesion, potentially further improving T cell expansion and function.

Several methods can be used to quantify antibody density on synthetic cells. We employed a calibration bead-based reagent kit, where fluorescently labeled beads with known ligand densities allow for FACS-based quantification of surface-bound antibodies<sup>10</sup>. Additionally, dissolving synthetic cells and performing ELISA assays provides an alternative approach to measure total antibody concentration in solution. Alternatively, dissolving synthetic cells followed by ELISA provides a way to measure total antibody content in solution. These techniques help establish the relationship between ligand density and T cell activation, guiding further protocol optimization. We found that antibody density can be tuned in a near-linear manner by titrating the input concentration during conjugation<sup>27</sup>; for example,

# Protocol

using 3×, 1×, 0.5×, 0.1× and 0.05× the standard amount (Table 3). As the antibodies used in this protocol have similar molecular weights and conjugation efficiencies, their relative composition can also be adjusted by simply changing the input ratios. This flexibility enables precise control over the anti-CD3: anti-CD28 ratio or incorporation of additional costimulatory signals. While our current protocol employs a 1:1 ratio, the optimization of ligand composition such as varying this ratio is an area of ongoing investigation. For larger or structurally diverse proteins, further optimization and quantification may be necessary to ensure consistent surface modification. By enabling precise control over ligand density and composition, this protocol provides a tunable platform for investigating the optimal conditions for T cell activation and offers potential advantages over traditional activation methods. To further improve ligand orientation and functional availability, alternative conjugation strategies such as antibodies with a biotinylated C-terminus of the Fc region bound to streptavidin-functionalized beads can be used. This approach offers directional control, ensuring that the antigen-binding (Fab) regions face outward, thereby enhancing TCR engagement efficiency. Future studies could systematically evaluate the impact of ligand ratios and additional costimulatory molecules to further enhance synthetic cell-mediated T cell activation.

While the ligand presentation on synthetic cells is precisely controlled, a direct comparison with Dynabeads remains challenging owing to the proprietary nature of their surface chemistry and antibody composition. Dynabeads are commercially optimized products, but their exact antibody ratio and composition remain unknown. In our previously published work, we attempted to quantify the antibody composition of Dynabeads using a fluorescence-based detection system<sup>27</sup>. Our results suggest that the anti-CD3: anti-CD28 ratio is not 1:1, but closer to 3:1, although it remains unclear whether anti-CD3 or anti-CD28 is more abundant. On the basis of prior studies, it is likely that anti-CD28 is in excess, as excessive anti-CD3 stimulation can lead to T cell anergy<sup>75</sup>.

## Controls

Comparative studies with conventional activators, such as Dynabeads, TransAct and pulsed moDC, are partially included as controls to benchmark the efficacy of synthetic cells. These controls allow for assessment of expansion rates, T cell phenotype and functionality, helping researchers evaluate the relative advantages of using synthetic cells.

## Safety

Safety is a priority, with synthetic cells designed for efficient removal after activation. Nontoxic, biocompatible materials are used to minimize potential cytotoxic effects, and all components can be safely separated from T cells postactivation to prevent carryover<sup>76–78</sup>.

## Separation

The protocol includes steps for removing synthetic cells from T cells following activation, using either simple centrifugation or chemical dissolution. Centrifugation ensures high cell purity and minimizes the risk of contamination, facilitating downstream applications such as *in vivo* infusions or further manipulations. As an alternative to physical separation, viscoelastic synthetic cells can also be separated by a calcium chelation method to break down the ionic crosslinking of alginate polymer. By introducing trace amounts of EDTA, the synthetic cells can be rapidly and almost instantaneously dissolved. This process produces alginate monomers as byproducts, which we have quantified by HPLC and found to be less than 50 ng/ml in the supernatant<sup>27</sup>. This low level of alginate had no detrimental effects on T cells in our experiments, consistent with findings from previous *in vitro* and *in vivo* studies<sup>77,79</sup>.

## Batch-to-batch consistency

Achieving consistent mechanical and biochemical properties across batches is essential for reproducibility. This protocol incorporates rigorous quality control measures to monitor properties such as size, ligand density and mechanical characteristics, ensuring uniformity across different batches of synthetic cells.

---

# Protocol

---

## T cell source

This protocol is compatible with T cells derived from various sources, including peripheral blood mononuclear cells (PBMCs) from healthy donors or pan T cells isolated from PBMCs. It has been shown that directly activating whole PBMCs yields comparable outcomes to activating isolated CD3<sup>+</sup> T cells in terms of both final cell product quality and T cell yield, with no clear differences observed<sup>27</sup>. However, for certain applications, it may be preferable to isolate CD3<sup>+</sup> T cells or CD8<sup>+</sup> T cells before activation for more targeted experimental needs.

## Synthetic cell dose

In static culture, synthetic cells are added to T cells at a 1:1 ratio, following a standardized approach to ensure consistency across experiments. Variations in the synthetic cell-to-T cell ratio can influence activation signal strength, T cell exhaustion and stemness retention. However, optimization of this ratio is beyond the scope of this protocol. To minimize potential discrepancies caused by experimental setup, a 1:1 ratio is consistently applied across all activator products used, ensuring reliable comparison of activation effects.

## Synthetic cell shelf life

The degradation of synthetic cells primarily results from the gradual breakdown of metal coordination bonds and polymer chains in aqueous environments, which can be influenced by factors such as pH and temperature. Experimental results indicate that synthetic cells retain stable surface ligand fluorescence for at least 60 d under refrigerated conditions, with no observed decline in signal intensity. However, extended storage may increase the risk of antibody detachment from the surface. Further research is needed to optimize long-term storage conditions, such as the use of glycerol–glucose solutions as cryoprotectants or freeze-drying methods, but these are beyond the scope of this protocol.

---

## Materials

---

### Biological materials

#### Human PBMCs

Healthy donor PBMCs were obtained from the UCLA/CFAR Virology Core Laboratory without identification information under federal and state regulations. Upon receipt, PBMCs were divided into aliquots of  $1-5 \times 10^7$  cells per vial and cryopreserved in liquid nitrogen for long-term storage.

▲ **CAUTION** Any experiments using human material must conform to relevant institutional and national regulations, and informed consent must be obtained.

▲ **CAUTION** Long-term storage of PBMCs at  $-80^\circ\text{C}$  is not recommended. PBMCs can be frozen and thawed multiple times, with up to three cycles generally considered acceptable.

#### Cell lines

The cell lines used in this protocol include various human tumor cell lines sourced from established repositories. For hematologic malignancies, the Burkitt's lymphoma cell line RAJI (RRID:CVCL\_0511) and the acute lymphoblastic leukemia cell line NALM6 (RRID:CVCL\_UJ05) were obtained from the American Type Culture Collection (ATCC). For solid tumors, we utilized ovarian cancer cell lines OVCAR3 (RRID:CVCL\_0465) and OVCAR8 (RRID:CVCL\_1629), pancreatic cancer cell line ASPC1 (RRID:CVCL\_0152), lung cancer cell line H226 (RRID:CVCL\_1544) and breast cancer cell line HCC1806 (RRID:CVCL\_1258), all sourced from ATCC.

▲ **CAUTION** The cell lines used in our research were regularly monitored to ensure their authenticity and to confirm that they are not infected with mycoplasma. None of the cell lines utilized in this study are known to be misidentified or cross-contaminated.

## Reagents

### Antibodies

- Purified anti-human CD3 antibody (clone OKT3, BioLegend, cat. no. 317302, RRID: [AB\\_571927](#))
- Fluorescein isothiocyanate (FITC) anti-human CD3 antibody (clone OKT3; BioLegend, cat. no. 317306, RRID: [AB\\_571907](#))
- Purified anti-human CD28 antibody (clone CD28.2, BioLegend, cat. no. 302902, RRID: [AB\\_314304](#))
- Anti-human CD3 (clone HIT3a, Pacific blue-conjugate, 1:500 dilution; BioLegend, cat. no. 300330, RRID: [AB\\_10551436](#))
- Anti-human HLA-DR, DP, DQ (clone Tü 39, PE/Cyanine7-conjugate, 1:250 dilution; BioLegend, cat. no. 361707, RRID: [AB\\_2564278](#))
- Anti-human CD45RO (clone UCHL1, APC-conjugate, 1:500 dilution; BioLegend, cat. no. 983102, RRID: [AB\\_2650651](#))
- Anti-human CD58 (clone TS2/9, PE-conjugate, 1:300 dilution; BioLegend, cat. no. 981702, RRID: [AB\\_3083238](#))
- Anti-human CD11a (clone TS2/4, FITC-conjugate, 1:200 dilution; BioLegend, cat. no. 350604, RRID: [AB\\_10662904](#))
- Anti-human CD183 (clone G025H7, FITC-conjugate, 1:200 dilution; BioLegend, cat. no. 353740, RRID: [AB\\_2566023](#))
- Anti-human CD19 (clone HIB19, PE-Cyanine5-conjugate, 1:300 dilution; BioLegend, cat. no. 982418, RRID: [AB\\_3083240](#))
- Anti-human CD69 (clone FN50, Pacific Blue-conjugate, 1:200 dilution; BioLegend, cat. no. 310920, RRID: [AB\\_493667](#))
- Anti-human CD45RA (clone HII100, FITC-conjugate, 1:200 dilution; BioLegend, cat. no. 983002, RRID: [AB\\_2650650](#))
- Anti-human CD62L (clone DREG-56, APC-conjugate, 1:400 dilution; BioLegend, cat. no. 980706, RRID: [AB\\_3097278](#))
- Anti-human CD95 (clone DX2, PE-conjugate, 1:800 dilution; BioLegend, cat. no. 987102, RRID: [AB\\_3068068](#))
- Anti-human CD25 (clone BC96, FITC-conjugate, 1:500 dilution; BioLegend, cat. no. 302604, RRID: [AB\\_314274](#))
- Anti-human CD279 (clone A17188A, FITC-conjugate, 1:200 dilution; BioLegend, cat. no. 379205, RRID: [AB\\_2922605](#))
- Anti-human CD366 (clone F38-2E2, APC-conjugate, 1:500 dilution; BioLegend, cat. no. 345012, RRID: [AB\\_2561718](#))
- Anti-human FOXP3 (clone 206D, Pacific blue-conjugate, 1:800 dilution; BioLegend, cat. no. 320116, RRID: [AB\\_439801](#))
- Purified anti-mouse CD3 antibody (clone 17A2, BioLegend, cat. no. 100202, RRID: [AB\\_312659](#))
- Purified anti-mouse CD28 antibody (clone 37.51, BioLegend, cat. no. 102102, RRID: [AB\\_312867](#))
- FITC anti-mouse CD3 antibody (clone 17A2; BioLegend, cat. no. 100204, RRID: [AB\\_312661](#))
- Anti-mouse CD4 (clone GK1.5, FITC-conjugate, 1:300 dilution; BioLegend, cat. no. 100406, RRID: [AB\\_312691](#))
- Anti-mouse CD366 (clone B8.2C12, APC-conjugate, 1:100 dilution; BioLegend, cat. no. 134008, RRID: [AB\\_2562998](#))
- Anti-mouse CD197 (clone 4B12, PE-conjugate, 1:500; BioLegend, cat. no. 120106, RRID: [AB\\_389358](#))
- Anti-mouse CD25 (clone PC61, FITC-conjugate, 1:300; BioLegend, cat. no. 102006, RRID: [AB\\_312855](#))
- Anti-mouse CD44 (clone IM7, APC/Cyanine7-conjugate, 1:300; BioLegend, cat. no. 103028, RRID: [AB\\_830785](#))
- Anti-mouse CD95 (clone SA367H8, PerCP/Cyanine5.5-conjugate, 1:600; BioLegend, cat. no. 152610, RRID: [AB\\_2632905](#))

- Anti-mouse CD62L (clone MEL-14, PerCP-conjugate, 1:400; BioLegend, cat. no. 104433, RRID:AB\_10900262)
- Anti-mouse CD95 (clone SA367H8, PE/Cyanine7-conjugate, 1:500; BioLegend, cat. no. 152617, RRID:AB\_2910313)
- Anti-mouse Ly-6A/E (clone D7, PE/Cyanine5-conjugate, 1:800; BioLegend, cat. no. 108110, RRID:AB\_313347)
- Anti-mouse CD279 (clone 29F.1A12, FITC-conjugate, 1:300 dilution; BioLegend, cat. no. 135214, RRID:AB\_10680238)
- Anti-human TNF (ELISA, capture, BD Biosciences, cat. no. 551220, RRID:AB\_394098)
- Anti-human TNF (ELISA, detection, BD Biosciences, cat. no. 554511, RRID:AB\_395442)
- Anti-human Granzyme B (clone GB11, APC-conjugated, 1:1,000 dilution; Thermo Fisher Scientific, cat. no. GRB05, RRID:AB\_2536539)
- Anti-human Perforin (clone dG9, PE-Cy7-conjugated, 5 µL/test; Thermo Fisher Scientific, cat. no. 25-9994-42, RRID:AB\_2573574)
- Anti-human CD4 (clone OKT4, FITC-conjugated, 5 µL/test; Thermo Fisher Scientific, cat. no. 11-0048-42, RRID:AB\_1633390)
- Anti-human CD8 (clone SK1, PerCP-eFluor 710, 5 µL/test; Thermo Fisher Scientific, cat. no. 46-0087-42, RRID:AB\_1834411)
- Anti-human CD8 (clone SK1, APC-Cy7-conjugated, 5 µL/test; BD Biosciences, cat. no. 348793, RRID:AB\_400383)
- Anti-human IFN-γ (clone 4S.B3, PE-Cy7-conjugated, 0.125 µg/test; Thermo Fisher Scientific, cat. no. 25-7319-82, RRID:AB\_469682)
- Goat anti-mouse IgG (H+L), Alexa Fluor 488-conjugated, 2 µg/mL; Thermo Fisher Scientific, cat. no. A-11001, RRID:AB\_2534069)
- Goat anti-mouse IgG (H+L), Alexa Fluor 647-conjugated; Thermo Fisher Scientific, cat. no. A-21236, RRID:AB\_2535805)
- Goat anti-rabbit IgG (H+L), Alexa Fluor 488-conjugated; Thermo Fisher Scientific, cat. no. A-11008, RRID:AB\_143165)

## Culture components

- RPMI 1640 (Gibco, cat. no. 11875093)
- Dulbecco's modified Eagle's medium, high glucose (Gibco, cat. no. 11965118)
- Penicillin–streptomycin–glutamine (100×) liquid (Gibco, cat. no. 10378016)
- FBS, premium (Gibco, cat. no. A5670701)
- MEM non-essential amino acids solution (100×) (Gibco, cat. no. 11140050)
- HEPES buffer solution (1M) (Gibco, cat. no. 15630080)
- Sodium pyruvate (100 mM) (Gibco, cat. no. 11360)
- 2-Mercaptoethanol (50 mM) (Gibco, cat. no. 31350010)
- ▲ **CAUTION** Toxic and volatile. Handle in a fume hood with gloves and eye protection.
- Normocin (Invivogen, cat. no. NC9273499)
- Recombinant human IL-2 (PeproTech, cat. no. 200-02)
- Concentrated lentivirus encoding CAR construct (prepared as described in refs. 80,81)
- Poloxamer synperonic F108 (MilliporeSigma, cat. no. 07579-250G-F)
- Prostaglandin E2 (PGE2) (Cayman Chemical, cat. no. 14010).
- Glass-bottom confocal dish (MatTek, cat. no. P35G-1.5-14-C)

## Other reagents

- Purified streptavidin (cat. no. 280302, Biolegend)
- Poly-L-lysine hydrobromide (MilliporeSigma, cat. no. P6282)
- CryoStor CS5 cell cryopreservation medium (MilliporeSigma, cat. no. C2874)
- Phosphate-buffered saline (PBS) (1×) (Gibco, cat. no. 10010023)
- Sodium chloride (MilliporeSigma, cat. no. S3014)
- Tween-20 (MilliporeSigma, cat. no. P1379)
- Dulbecco's modified Eagle's medium (Gibco, cat. no. 11965118)
- GlutaMAX supplement (100×) (Gibco, cat. no. 35050061)

# Protocol

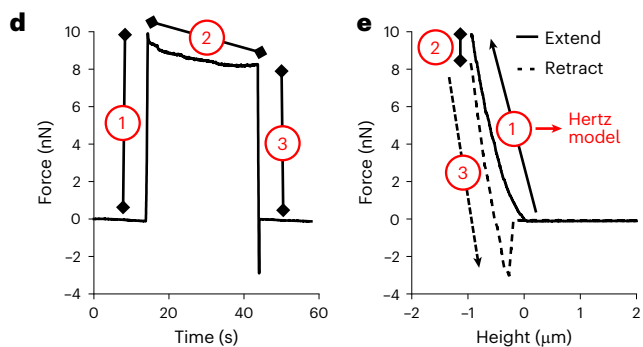
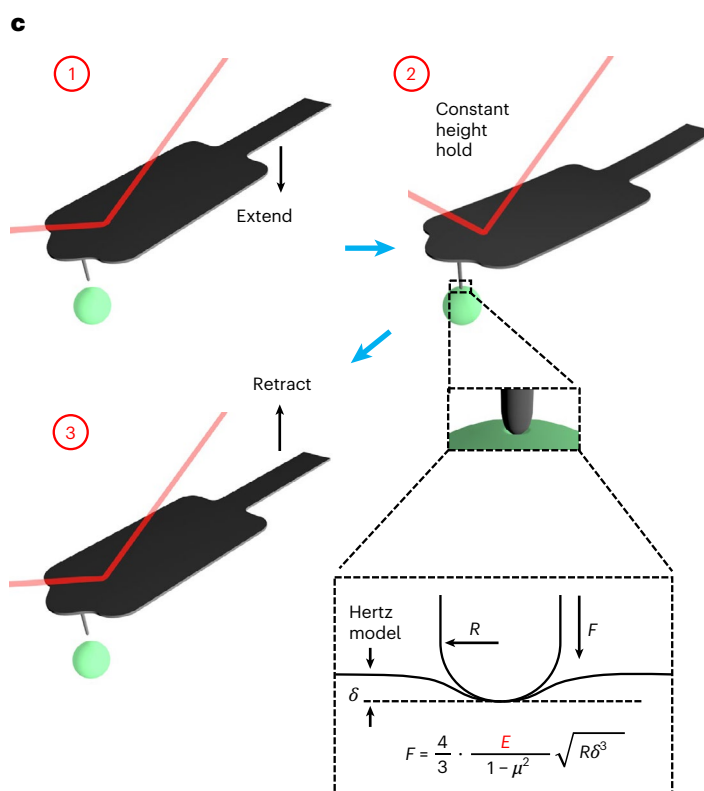
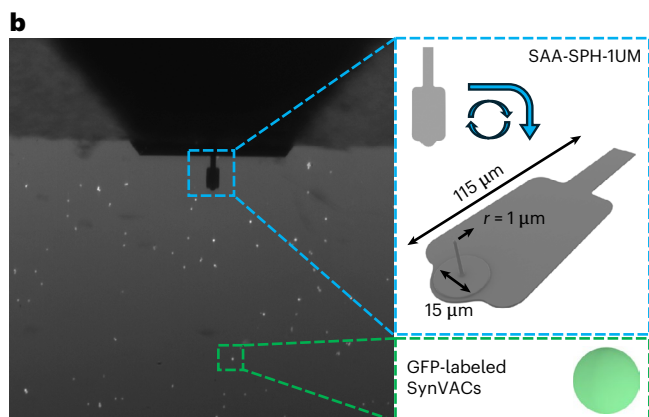
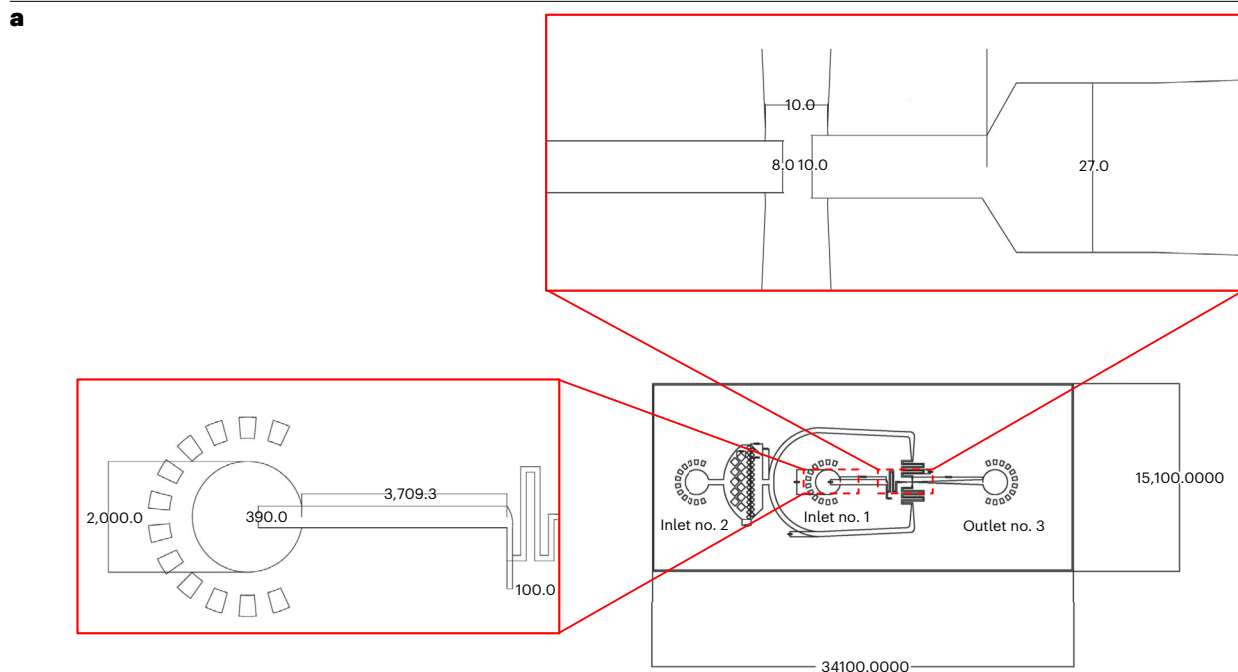
- HEPES (MilliporeSigma, cat. no. H4034)
- Streptavidin–HRP conjugate (Invitrogen, cat. no. SA10001)
- Quantum Simply Cellular kits (Bang labs, cat. no. 815A)
- IFN gamma ELISA kit (R&D Systems, cat. no. PDIF50C)
- TNF ELISA kit (Invitrogen, cat. no. KHC3011)
- IL-2 ELISA kit (Invitrogen, cat. no. BMS221-2)
- Micro BCA protein assay kit (Thermo Scientific, cat. no. 23235)
- CD14 MicroBeads kit (Miltenyi Biotec, cat. no. 130-118-906).
- DAPI and Hoechst nucleic acid stains (Thermo Fisher, cat. no. 62249)
- D-Luciferin (Caliper Life Science, cat. no. 119222)
  - ▲ **CAUTION** Light-sensitive and potentially irritating. Store protected from light and avoid skin contact.
- Fixable viability dye eFluor 506 (e506; eBioscience, cat. no. 65-0866-18)
- MES (MilliporeSigma, cat. no. M3671)
- TCO-PEG4-NHS Ester (BroadPharm, cat. no BP-22418)
- Tetrazine-PEG5-NHS (BroadPharm, cat. no BP-22681)
- EDC (MilliporeSigma, cat. no. 39391).
  - ▲ **CAUTION** Irritant and reactive. Avoid inhalation and skin contact; wear appropriate PPE.
- NHS (MilliporeSigma, cat. no. 130672)
  - ▲ **CAUTION** Irritant; avoid inhalation or prolonged skin exposure.
- Glucose monohydrate (MilliporeSigma, cat. no. Y0001745)
- Potassium chloride (MilliporeSigma, cat. no. P3911)
- Calcium chloride (MilliporeSigma, cat. no. C5670)
- SYLGARD 184 silicone elastomer kit (Dow)
  - ▲ **CAUTION** May cause skin or eye irritation; handle with gloves.
- PRONOVA UP VLVG (MilliporeSigma, cat. no. 42000501)
- PRONOVA UP MVG (MilliporeSigma, cat. no. 42000101)
- Ethylenediaminetetraacetic acid calcium disodium salt hydrate (MilliporeSigma, cat. no. 340073)
- (MilliporeSigma, cat. no. 340073)
- Sodium carboxymethyl cellulose (CMC; MilliporeSigma, cat. no. 419303)
- 3M Novec 7500 engineered fluid (3M, cat. no. 7100025016)
  - ▲ **CAUTION** Fluorinated fluid; avoid inhalation of vapor; ensure good ventilation.
- Acetic acid (MilliporeSigma, cat. no. 01-0310)
  - ▲ **CAUTION** Flammable and corrosive. Use in fume hood; avoid skin and eye contact.
- Viscosity oil, 157 FSH (Grainger, cat.no. NC2010825)
- 1H,1H,2H,2H-Perfluoro-1-octanol (MilliporeSigma, cat. no. 370533)
  - ▲ **CAUTION** Combustible. Please use it in a chemical fume hood.

## Equipment

### Equipment for synthetic cell generation

- Oxygen plasma cleaner (for example, Harrick Plasma, model no. PDC-32G or equivalent)
- Hot plate with digital temperature control (Corning, model no. PC-400D or equivalent)
- MA6 mask aligner (SUSS MicroTec)
- Spin coater (Laurell Technologies, model no. WS-650-23NPP or equivalent)
- Autoclave (for example, Tuttnauer, model no. 3870M or equivalent)
- High-speed centrifuge (for example, Eppendorf, model no. 5810R)
- Cleanroom workbench (for example, Class 100 laminar flow bench, Baker Company)
- Precision micropipettes (for example, Gilson PIPETMAN Classic, P20, P200, P1000)
- Conical tubes (15 mL and 50 mL) (for example, Corning, cat. nos. 430790 and 430828)
- Standard infusion only pump 11 Elite Syringe Pumps (HARVARD Apparatus, cat. no. 70-4500)
- Microcentrifuge tubes: 2.0 mL (Fisher Scientific, cat.no. 05-408-138)
- 3D-printed microbead collector (custom-designed funnel-shaped collector compatible with outlet #3 dimensions. Used for periodic collection of microbead-containing emulsions during droplet generation. STL file or design specifications available upon request)

# Protocol



## Equipment for click chemistry

- Orbital shaker (for example, Thermo Fisher Scientific, model no. 4625 or equivalent)
- UV-visible spectrophotometer (for example, Shimadzu, model no. UV-1800)
- Microplate reader (for example, Tecan Infinite M Nano)
- Magnetic stirrer with hot plate (IKA, model no. C-MAG HS 7 or equivalent)
- Refrigerated centrifuge (for example, Thermo Scientific Sorvall ST 16R)

**Fig. 3 | The engineering design of the microfluidic chip used in this protocol and mechanical characterization of synthetic cells.**

**a**, Inlet no. 1 corresponds to the entry point for the alginate solution, inlet no. 2 corresponds to the entry point for the oil phase and outlet no. 3 is the exit point for the microbeads. The magnified section shows the dimensions of the junction where the different liquid phases meet, with all measurements in micrometers. **b**, AFM characterization of viscoelasticity and stiffness of GFP-labeled synthetic cells. Visualization of GFP-labeled synthetic cells and the AFM cantilever under the JPK NanoWizard 4a BioScience AFM system. **c**, A schematic representation of the AFM probe interacting with GFP-labeled synthetic cells, highlighting three key stages of the indentation process: (1) the probe extends toward the synthetic

cell and makes contact; (2) the probe holds at a constant height to allow stress relaxation measurement; and (3) the probe retracts from the synthetic cell. The indentation data are fitted to the Hertz model to determine stiffness. Parameters:  $F$  (applied force),  $R$  (probe radius),  $\delta$  (sample indentation),  $E$  (Young's modulus) and  $\mu$  (Poisson's ratio). **d**, Stress-relaxation data corresponding to the three phases of indentation, showing the force–time relationship during approach (1), hold (2) and retraction (3) to characterize the viscoelastic properties of the synthetic cells. **e**, Application of the Hertz model to the approach (extension) phase (1) of the force–height relationship to determine Young's modulus, with relaxation (2) and retraction (3) phases also indicated.

- Syringe filters (0.2  $\mu\text{m}$  PES and Nylon membranes) (for example, Millex, cat. nos. SLGP033RS and SLGN033NS)
- Biological safety cabinet (for example, Baker Company, Sterilgard Series)
- CO<sub>2</sub> incubator (5% CO<sub>2</sub>, 37 °C, 90% humidity, for example, Thermo Fisher Scientific, Heracell 240i)
- Confocal microscope (for example, Zeiss LSM 900 with Airyscan)
- Cryogenic vials (for example, Thermo Fisher Scientific, cat. no. 375418)
- Ultralow temperature freezer (–80 °C) (for example, Panasonic VIP ECO Series)
- Automated cell counter (for example, Bio-Rad, model no. TC20 or Countess II)
- Flow cytometer (for example, BD FACSCanto II or MACSQuant Analyzer 10, Miltenyi Biotech)
- Bio-AFM system (for example, NanoWizard 4a BioScience AFM)
- Chromium platform for single-cell sequencing (for example, 10X Genomics Chromium Controller)
- Single-cell RNA sequencing (scRNA-seq) kits (for example, Chromium Next GEM Single Cell 3' Kit v3.1, 10X Genomics)
- Light microscope with camera (for example, Olympus CKX53)
- 70  $\mu\text{m}$  cell strainers (for example, Corning, cat. no. 431751)
- Centrifuge for 1.5 mL microtubes (for example, Eppendorf MiniSpin Plus)
- Ultralow attachment plates (6 well and 24 well) (for example, Corning, cat. nos. CLS3471 and CLS3473)
- Microscope slides and cover glasses (for example, Fisherbrand, cat. no. 12545C)

## Reagent setup

**Chrome mask for microfluidic fabrication:** a custom designed 4-inch chrome mask used for photolithography. Fabricated by the UCLA MASK SHOP with a recommended precision of 2  $\mu\text{m}$  and a tolerance of  $\pm 0.2 \mu\text{m}$ . The mask design includes critical features at the liquid–oil phase intersections, as shown in Fig. 3a.

**Alginate solution:** to prepare the alginate solution, first make the following stock solutions: 5 wt% very low viscosity grade (VLVG) alginate (molecular weight 70 kDa) in distilled water (can be stored at 4 °C for 3 month), 5 wt% carboxymethyl cellulose (CMC) in distilled water (can be stored at 4 °C for 3 month), 75 mM EDTA-Ca<sup>2+</sup> (V1) and 250 mM EDTA-Ca<sup>2+</sup> (V2) in distilled water (can be stored at 4 °C for 1 year). For dissolving alginate powder, the optimal method is to mix the alginate powder with distilled water in a 50 mL centrifuge tube and incubate the tube in a 37 °C water bath overnight. On the day of bead preparation using microfluidics or the day before, mix 0.75 mL of the 5% VLVG solution, 0.25 mL of the 5% CMC solution and either 0.25 mL of the 75 mM EDTA-Ca<sup>2+</sup> solution (V1) or 0.25 mL of the 250 mM EDTA-Ca<sup>2+</sup> solution (V2) thoroughly. Store the prepared water phase (can be stored at 4 °C for 1 week) in a well-sealed container if not used immediately to prevent drying or contamination.

This protocol primarily describes how the elastic formulations E1 and E2 are generated by applying a post-crosslinking process to the viscoelastic V1 microbeads. However, the same crosslinking strategy can also be applied to viscoelastic microbeads derived from alginates of different molecular weights (V2 or other formulations), as demonstrated in our previous work<sup>27</sup>.

To produce E1 (soft elastic) or E2 (stiff elastic) beads, first generate viscoelastic microbeads (V1) using the above method, then purify them as described in the Procedure

# Protocol

(fabrication Stage 2). After purification, resuspend the beads in MES-CT buffer and perform crosslinking using 50 mg/mL EDC, 3.5 mg/mL HoBt and 1.04 mg/mL AAD in MES-CT (E1) or 50 mg/mL EDC, 10 mg/mL HoBt and 5.2 mg/mL AAD in MES-CT (E2). Allow the crosslinking reaction to proceed overnight at room temperature (20–25 °C) in a sealed tube to prevent CO<sub>2</sub> buildup. After incubation, wash the beads thoroughly according to the protocol.

▲ **CRITICAL** CMC is used to adjust the viscosity of the solution to match the oil phase, which is crucial for maintaining the laminar flow stability in the microfluidic device. Proper viscosity matching improves bead formation efficiency and increases microbead yield.

**Oil phase solution:** to prepare 10 mL of the oil phase containing 7500 engineered fluid, 1 wt% FSH surfactant and 0.5% (v/v) acetic acid, begin by measuring 10 mL of 7500 engineered fluid into a clean, dry container and measure its weight. Add 1% 7500 engineering fluid weight of FSH surfactant to the oil and mix thoroughly to ensure the surfactant is evenly dispersed. Next, add 0.05 mL of acetic acid to the mixture. Stir the solution continuously using a magnetic stirrer or vortex mixer until a homogeneous oil phase is obtained. Ensure all components are well-incorporated and free from separation before use. The prepared oil phase should be used immediately or stored in a sealed container to prevent evaporation or contamination. The solution can be stored at room temperature for 1 month.

**Collection solution:** To prepare 10 mL of the solution containing 7500 engineered fluid, 10% (vol/vol) perfluorooctane and 0.2% (vol/vol) acetic acid, start by measuring 9 mL of 7500 engineered fluid into a clean, dry container. Add 1 mL of perfluorooctane to the engineered fluid and mix thoroughly using a magnetic stirrer or vortex mixer to ensure uniform dispersion. Next, add 0.02 mL of acetic acid to the mixture and continue stirring until a homogeneous solution is achieved. The solution can be stored at room temperature for 1 month. Verify that all components are well-incorporated without phase separation before proceeding.

**HEPES buffer:** to prepare the HEPES buffer solution, dissolve 5 g of HEPES in 1 L of distilled water in a clean container while stirring to ensure complete solubilization. Add 8 g of sodium chloride (NaCl) and mix until fully dissolved, followed by 0.37 g of potassium chloride (KCl) and 1.076 g of disodium phosphate (Na<sub>2</sub>HPO<sub>4</sub>), stirring thoroughly after each addition. Next, add 1 g of glucose and continue stirring until the solution is homogeneous. Adjust the pH to 7.4 by adding 0.5 M sodium hydroxide (NaOH) dropwise while continuously stirring and monitoring the pH with a calibrated pH meter. Once the pH reaches 7.4, the buffer is ready for use or can be stored at room temperature in a sealed container for up to 1 year.

**2-(*N*-Morpholino) ethanesulfonic acid (MES) buffer:** to prepare a buffer solution containing 0.1 M MES and 0.3 M NaCl, begin by dissolving 19.52 g of MES and 17.53 g of sodium chloride (NaCl) in ~900 mL of distilled water. Stir the solution thoroughly until both the MES and NaCl are completely dissolved. Adjust the pH of the solution to the desired value (typically between 5.5 and 6.7 for MES buffers) by adding 1 M NaOH dropwise while continuously stirring and monitoring the pH with a calibrated pH meter. Once the desired pH is reached, adjust the final volume to 1 L with distilled water. Filter the solution through a 0.22 μm filter for sterility, if required, and store at room temperature in a sealed container for up to 1 year.

▲ **CAUTION** Low hazard but irritating in dust form; use gloves and eye protection.

**Human T cell culture media:** to prepare the C10 human T cell culture media with additional supplements, start with RPMI 1640 as the base medium. Add 10% (vol/vol) heat-inactivated FBS to supply essential growth factors. Supplement the medium with 1% (vol/vol) penicillin–streptomycin for antibacterial protection, 2 mM L-glutamine to support cellular metabolism and 50 U/mL recombinant human interleukin-2 (IL-2) to promote T cell activation and expansion. Incorporate 1% (vol/vol) MEM non-essential amino acids to provide additional nutrients that enhance cell survival and function. Add normocin (at the manufacturer-recommended concentration) to protect against mycoplasma, bacterial and fungal contamination. Filter the complete media through a 0.22 μm filter for sterility. Store the prepared medium at 4 °C for up to 6 months and warm it to 37 °C before use.

**Dual-reporter tumor cell lines:** to enable bioluminescence and fluorescence-based detection in the tumor killing assay, tumor cell lines (for example, RAJI, OVCAR3, OVCAR8, ASPC1, H226 and HCC1806) were transduced with lentiviral vectors encoding a dual-reporter construct consisting of firefly luciferase (Fluc) and enhanced green fluorescent protein (eGFP). Following

# Protocol

transduction, cells were sorted by flow cytometry to isolate successfully transduced populations, which were expanded and used as stable dual-reporter lines in downstream cytotoxicity assays.

**APCs:** APCs used in this protocol are primary monocytes extracted from human PBMCs using the CD14 MicroBeads kit. Isolate PBMCs through density gradient centrifugation, followed by magnetic cell sorting to enrich CD14<sup>+</sup> monocytes. These isolated APCs are used for atomic force microscopy (AFM) measurements to assess their mechanical properties, rather than for antigen presentation (Step 78A). The use of primary APCs in AFM studies ensures that the mechanical characteristics measured are physiologically relevant, providing insights into their role in immune cell interactions.

**Ethanol mixture (70% vol/vol):** measure 737 mL of 190-proof ethanol into a 1 L graduated cylinder. Add ultrapure water to bring the total volume to 1 L. Transfer the mixture to a sealed container or spray bottle and store at room temperature for up to 1 year.

**▲ CAUTION** Ethanol is highly flammable and can cause respiratory irritation if inhaled. Keep away from open flames and work in a well-ventilated area.

## Procedure

**▲ CRITICAL** In this protocol, all referenced day numbers (for example, day 1) denote the specific days within that procedure. Each section outlines day numbers starting from day 0.

### Fabrication Stage 1: manufacture of device and microbeads

#### ● TIMING 5 d

- On day 0 (fabrication Stage 1), inspect the chrome mask to verify that all critical features, especially at the liquid–oil phase intersections (Fig. 3a), match the design with dimensional deviations of less than 0.2  $\mu\text{m}$ . Use high-resolution microscopy or profilometry as appropriate to assess pattern fidelity. Chrome masks can be outsourced to professional micro/nano fabrication facilities.  
**▲ CRITICAL STEP** Precise alignment and fidelity of the chrome mask are essential for reliable microfluidic channel formation. Deviations greater than 0.2  $\mu\text{m}$  can compromise droplet formation and flow stability.
- On day 1, clean a 4-inch silicon wafer with acetone and isopropanol (IPA), then dry with nitrogen gas.  
**▲ CRITICAL STEP** Only remove wafers from their container in the cleanroom to avoid oxidation and contamination of unused wafers.
- Apply SU-8 2015 photoresist onto the silicon wafer and spin-coat using the following parameters: spin speed 3,500 rpm for 60 s, achieving a film thickness of ~13  $\mu\text{m}$ .  
**▲ CRITICAL STEP** The spin-coating thickness determines the height of the microfluidic channels. An acceptable thickness range for SU-8 2018 is 12–15  $\mu\text{m}$ , as deviations beyond this range may impact microchannel dimensions and flow dynamics (Table 4). According to the official SU-8 2018 technical datasheet, thicknesses within 6–15  $\mu\text{m}$  follow the same

**Table 4 | Microfluidic fabrication parameters**

Step	Parameter	Value
Step 1: SU-8 2015 spin coating	Spin speed	3,500 rpm
	Film thickness	13 $\mu\text{m}$
Step 2: exposure	Irradiance	20 mW/cm <sup>2</sup>
	Exposure time	15 s
Step 3: baking	Soft bake conditions	3 min at 95 °C: gradual ramp up/down
	Post bake conditions	6 min at 95 °C: gradual ramp up/down
	Hard bake conditions	30 min at 150 °C

bake time and exposure dose, indicating that minor variations within this range do not compromise fabrication consistency. Maintaining a thickness of at least 12  $\mu\text{m}$  ensures that the microchannel is sufficiently high to prevent compression of the beads during fabrication and operation.

▲ **CRITICAL STEP** To confirm that the SU-8 2015 film thickness is  $\sim 13 \mu\text{m}$ , researchers can use noncontact measurement techniques such as ellipsometry or reflectometry, which allow precise thickness determination without damaging the resist layer. If direct measurement is not feasible, consistency can be ensured by strictly following the spin-coating parameters specified in the datasheet.

4. Perform soft baking on a hot plate at 65 °C for 1 min, followed by 95 °C for 3 min, then allow to cool gradually.
5. Align the chrome mask onto the photoresist-coated wafer using a mask aligner and expose the wafer to UV light (20 mW/cm<sup>2</sup>) for 15 s.

▲ **CRITICAL STEP** It is recommended to use a mask aligner with VAC (vacuum contact) mode. Regular hard contact mode may increase fabrication errors.

6. Post-bake the wafer on a hot plate at 65 °C for 1 min, then at 95 °C for 6 min and then gradually cool.
7. Immerse the wafer in SU-8 developer solution and gently agitate for 3–4 min to remove unexposed photoresist. Rinse the wafer with IPA and inspect it under a microscope to ensure the pattern matches the design.

▲ **CRITICAL STEP** Ensure that critical features of the fabricated chrome mask, especially at the liquid–oil phase intersections, have deviations of less than 0.5  $\mu\text{m}$  from the chrome mask.

#### ◆ **TROUBLESHOOTING**

8. Hard-bake the developed wafer on a hot plate at 150 °C for 30 min to stabilize the structure.
9. Place the mold in a vacuum desiccator with 100–200  $\mu\text{L}$  of trichlorosilane solution (1–5% in anhydrous ethanol or isopropanol) and maintain a vacuum ( $\sim 20$ –50 mTorr). Allow the silanization to proceed for 12–16 h.
10. After treatment, carefully vent the desiccator, rinse the mold with ethanol or isopropanol to remove unreacted silane and dry thoroughly before use. This hydrophobic treatment ensures easy separation of PDMS during replica molding.

▲ **CRITICAL STEP** Ensure the SU-8 mold is completely clean and dry before silanization, as any residual moisture can interfere with the reaction.

▲ **CRITICAL STEP** To confirm successful hydrophobic treatment, perform a water contact angle measurement. A well-silanized SU-8 mold should exhibit a contact angle  $>100^\circ$ , indicating strong hydrophobicity. If the treatment is successful, a drop of deionized water placed on the surface should bead up rather than spread. If the water droplet spreads, the mold may require resilanization or extended reaction time to achieve optimal surface modification.

11. On day 2, weigh 25 g of PDMS part A and 2.5 g of part B using an analytical scale.
12. Mix the PDMS components thoroughly using a glass rod for 5 min. Ensure the mixture is homogeneous and free of streaks to guarantee even distribution of both components.

▲ **CRITICAL STEP** All PDMS handling should be done carefully to avoid contamination or improper curing.

13. Retrieve the silanized SU-8 mold and prepare a disposable container using aluminum foil. Shape the foil into a bowl-like structure (like origami), ensuring the SU-8 mold is securely positioned at the bottom. Minimize the gap between the bottom of the SU-8 mold and the aluminum foil to provide a snug fit and prevent leakage.
14. Pour the thoroughly mixed PDMS (25 g of part A and 2.5 g of part B) into the prepared container.
15. Place the container under a vacuum for 20–30 min to remove any air bubbles trapped in the PDMS mixture.

▲ **CRITICAL STEP** The volume of the poured PDMS mixture determines the overall height of the microfluidic chip. Typically, a final chip thickness of  $\sim 4 \text{ mm}$  is ideal. Adjust the total amount of PDMS mixture prepared based on the specific requirements of the application. If the chip is too thin ( $<3 \text{ mm}$ ), the high internal pressure may cause the tubing to dislodge during operation, leading to fluid leakage and requiring chip replacement. A thicker PDMS layer improves mechanical stability but results in additional material usage.

# Protocol

16. Place the mold containing the PDMS mixture into an oven and heat at 65 °C for 30–60 min to allow it to fully cure. After curing, store the mold in a dry, room-temperature environment overnight before proceeding with the peel-off step.
  - ▲ **CRITICAL STEP** Allowing the PDMS to sit for an extended period improves mechanical stability and adhesion balance, making the peel-off process easier and reducing the risk of structural damage. Avoid storing the mold in humid conditions as residual moisture may interfere with successful demolding.
17. On day 3, carefully peel off the mold and meticulously apply Magic tape (3M 810 Scotch) to all surfaces of the microfluidic channel.
  - ▲ **CRITICAL STEP** The tape enhances the visibility of the microfluidic channels. Without it, the transparent PDMS makes it difficult to locate the individual chip boundaries, complicating subsequent cutting.
  - ◆ **TROUBLESHOOTING**
18. Use a scalpel to cut individual chips from the cured PDMS block. Typically, a 4-inch mold can yield up to 8 individual chips.
19. Use biopsy punches of appropriate dimensions to create inlet and outlet holes on the chip. Punch inlet #1 and inlet #2 using a 2 mm biopsy punch, and punch outlet #3 using a 3.5 mm biopsy punch according to our design specifications in Fig. 3a.
  - ▲ **CRITICAL STEP** It is recommended to punch from the microchannel side of the chip to ensure a tighter fit when connecting silicone tubing later.
20. Sequentially clean PDMS chips and glass slides of matching dimensions using a 70% ethanol mixture and deionized water via ultrasonication. Perform each cleaning cycle for 20 min and repeat the process twice. Finally, air-dry the surfaces in a biosafety cabinet, ensuring that the surfaces intended for bonding are facing upward.
21. On day 4, subject the chips and glass slides to plasma treatment using a plasma cleaner under the following conditions: power set to 18 W and pressure at ~200 mTorr for 28 s. Ensure the chamber is properly vented before and after the treatment to maintain consistency in the process.
  - ▲ **CRITICAL STEP** It is best to process one chip and one glass slide at a time and then process the next batch after they have been successfully bonded, to prevent the effect of plasma from weakening over time and causing bonding failure.
22. Place the PDMS chips on glass slides with the microfluidic channel side facing the glass slide. Incubate the bonded devices at 65 °C overnight to allow deplasma recovery and restore hydrophobicity. Seal the device surfaces with tape to prevent dust contamination.
  - ▲ **CRITICAL STEP** During the bonding process, gently press the PDMS with your fingers, but avoid applying excessive pressure as this may cause microfluidic channel closure.
  - **PAUSE POINT** The devices can be stored at room temperature until being used for making microbeads.
  - ◆ **TROUBLESHOOTING**
23. On day 5, remove the microfluidic device from the incubator, remove the surface tapes and place it under the objective of an inverted microscope. Connect a syringe loaded with 1 mL of alginate solution to inlet 1 and a syringe containing the oil phase liquid to inlet 2.
  - ▲ **CRITICAL STEP** Depending on the molecular weight of the alginate used, the prepared beads are categorized into two types of viscoelastic microbeads: V1 and V2 (Table 3).
  - ▲ **CRITICAL STEP** Manually purge air from the silicone tubing in advance, filling it with solution. This step can save considerable time. When connecting the silicone tubing to the device inlets, leave some space for air at the connection point to prevent excessive solution from being squeezed into the microfluidic channel during insertion, which could cause channel blockage.
24. Drive the alginate solution at 300  $\mu\text{L}/\text{h}$  until it reaches the cross-junction of the liquid and oil phases (Fig. 3a). Then stop the alginate solution injection pump. Push the oil phase at 500  $\mu\text{L}/\text{h}$ . When the oil phase reaches the alginate solution position, immediately drive the alginate solution at 100  $\mu\text{L}/\text{h}$ .
  - ▲ **CRITICAL STEP** The purpose of this operation is to prevent the alginate solution from entering the oil phase channel before the oil phase arrives, or vice versa. After initiating

# Protocol

alginate flow at 100  $\mu\text{L}/\text{h}$ , do not immediately adjust the oil phase parameters. Instead, observe under a microscope whether microbeads begin forming at the cross-junction. If microbeads are visible, this indicates that the pressure balance between the alginate and oil phases is optimal. Once confirmed, proceed to the next step as described.

## ◆ TROUBLESHOOTING

25. Once the fluid stabilizes, set the alginate solution flow rate to 18  $\mu\text{L}/\text{h}$  and the oil phase flow rate to 300  $\mu\text{L}/\text{h}$ . Simultaneously, insert the 3D-printed collector into outlet #3 of the microfluidic device. Collect samples approximately every 6 h by transferring the emulsion from the collector into a preprepared 0.5 mL collection fluid in a microcentrifuge tube. The total collection duration can be adjusted based on the desired quantity of microbeads. This interval ensures that the microbeads concentration in the collection tube remains within an optimal range, preventing excessive accumulation or overly diluted samples. Maintaining an appropriate microbeads density facilitates efficient downstream separation and processing without requiring additional concentration or dilution steps.  
**▲ CRITICAL STEP** The collector can be designed with a simple funnel shape, ensuring that its bottom matches the dimensions of outlet #3 for easy insertion. The collection frequency depends on the volume design of the collector.
26. Add 0.7 mL of HEPES-CT to 0.5 mL of the collected samples in a microcentrifuge tube. Centrifuge at 1,500g for 1.5 min.  
**▲ CRITICAL STEP** After centrifugation, the microbeads, being a highly hydrated hydrogel, have a lower density than the fluorinated oil, causing them to leave the oil phase and enter the aqueous phase. At this point, most microbeads are suspended above the oil–water interface.  
**■ PAUSE POINT** Collected samples can be stored at 4 °C for up to 1 week before proceeding to purification.

## Fabrication Stage 2: processing of microbeads

### ● TIMING 1–2 d

27. On day 0 (fabrication Stage 2), prepare MES buffer and HEPES-CT as specified in the following table.

Buffer type	Base buffer	CaCl <sub>2</sub> concentration	Tween-20 concentration
MES-CT	MES buffer (pH 6)	2 mM	0.5%
HEPES-CT	HEPES buffer (pH 7.4)	2 mM	0.5%

28. Gently collect the top 0.5 mL of the buffer from the samples collected in Step 26 without disturbing the water–oil interface.  
**▲ CRITICAL STEP** Use a pipette tip between 200 and 1,000  $\mu\text{L}$  when collecting the top aqueous phase. Tips smaller than 200  $\mu\text{L}$  may generate excessive shear force that can damage the microbeads. Regardless of tip size, take care not to disturb the water–oil interface while aspirating the buffer. To maximize recovery, aspirate as much of the buffer above the oil as possible without disrupting the interface. This step requires some practice to perform reliably.
29. Add another 0.5 mL of HEPES-CT buffer to the tube and centrifuge at 1,500g for 1.5 min. Collect the top 0.5 mL of the HEPES buffer. Repeat the washing step two to four times. Performing additional washes can improve microbead recovery, but two washes are generally sufficient for most applications.
30. (Optional) Steps 30–33 describe the process of converting viscoelastic microbeads (V1) into elastic microbeads (E1/E2). If only viscoelastic microbeads are required, please proceed to Step 34. If converting V1 to E1/E2, centrifuge the microbeads at 6,000g for 5 min. Gently aspirate and discard the top 1.5 mL of the supernatant. Add 1.5 mL of MES-CT buffer to the microcentrifuge tube.  
**▲ CRITICAL STEP** Although this protocol uses V1 as the representative formulation, other viscoelastic bead types can also be used for conversion to E1/E2 with minor adjustments to the crosslinking parameters<sup>27</sup>.

**Table 5 | Summary of materials and reagents for antibody modification with tetrazine**

Protein Type	Molecular weight	Tetrazine reagent	Reagent concentration	Reaction buffer	Incubation time	Purpose of modification
Anti-CD3	150 kDa	Tetrazine-PEG4-NHS	30–60 $\mu$ M	HEPES (pH 8.4)	45 min at room temperature	T cell activation
Anti-CD28	150 kDa	Tetrazine-PEG4-NHS	30–60 $\mu$ M	HEPES (pH 8.4)	45 min at room temperature	Costimulatory signal
Mesothelin	33 kDa	Tetrazine-PEG4-NHS	60 $\mu$ M	HEPES (pH 8.4)	45 min at room temperature	Antigen-specific activation
Anti-CD3-FITC	150 kDa	Tetrazine-PEG4-NHS	30–60 $\mu$ M	HEPES (pH 8.4)	45 min at room temperature	Ligand density quantification

31. (Optional) Repeat the previous step. Centrifuge the microbeads again at 6,000g for 5 min, then gently aspirate and discard the top 1.5 mL of the supernatant.
32. (Optional) To prepare crosslinking solutions A and B for 1 million microbeads, adjust the formulation based on the desired stiffness of the elastic microbeads. If higher stiffness is desired, the concentrations of HoBt and AAD can be proportionally increased while keeping the EDC concentration constant, as it is already in excess.

Solution	Base buffer	EDC (mg/mL)	HoBt (mg/mL)	AAD (mg/mL)	Target product
Crosslinking solution A	MES-CT	50	3.5	1.04	E1
Crosslinking solution B	MES-CT	50	10	5.2	E2

▲ **CRITICAL STEP** When mixing the crosslinking solution, note that the EDC reaction releases CO<sub>2</sub> gas as a byproduct. Make sure the microcentrifuge tube is tightly sealed to prevent the cap from popping open during incubation.

33. (Optional) Combine 1 million microbeads with 400  $\mu$ L of the appropriate crosslinking solution and mix thoroughly. React overnight at room temperature.
34. Count the number of microbeads using a hemocytometer.

■ **PAUSE POINT** Store the microbeads at 4 °C in HEPES-CT for up to 1 month.

◆ **TROUBLESHOOTING**

### Fabrication Stage 3: surface chemistry

● **TIMING** 4 d

▲ **CRITICAL** This stage requires precise temperature control and strict adherence to centrifugation times to ensure the integrity and functionality of the antibodies. Ensure all centrifugation steps are done at 3,500g to properly pass the antibody through the column without causing damage or loss of material.

▲ **CRITICAL** Preparation of buffers and handling of antibodies should be performed under sterile conditions to prevent contamination.

35. On day 0 (fabrication Stage 3), prepare the ultrafiltration column by washing it with 2 mL of HEPES buffer and centrifuging at 3,500g for 10 min. Discard the filtrate collected in the tube.
36. Load the column with the antibody or protein solution of interest (Table 5) and centrifuge at 3,500g for 15 min at room temperature. Discard the filtrate in the collection tube.
 

▲ **CRITICAL STEP** Different antibodies may be conjugated together in a single reaction, as they typically have similar molecular weights and conjugation behavior. An example of such an antibody mixture is provided below.

Solution	Base buffer	Anti-CD3 ( $\mu$ M)	Anti-CD28 ( $\mu$ M)	Molar ratio	Total volume ( $\mu$ L)
Single antibody (CD3)	PBS	5–10	–	–	200
Single antibody-FITC (CD3)	PBS	5–10	–	–	200
Single antibody (CD28)	PBS	–	5–10	–	200
Antibody mixture	PBS	5–10	5–10	1:1	200

# Protocol

37. Immediately after loading, wash the column three times with 2 mL of HEPES buffer (pH 8.4). For each wash, centrifuge at 3,500g for 15 min and discard the filtrate.
38. Measure the antibody or protein concentration using a NanoDrop spectrophotometer, using HEPES buffer (pH 8.4) as the blank. While NanoDrop is generally suitable for both antibodies and proteins, we recommend confirming protein concentrations with a micro BCA assay.
39. Add 10 mmol/L of tetrazine-PEG5-NHS-ester to the antibody solution at a molar ratio of 1:6 (antibody to tetrazine). Wrap the container in foil to protect it from light and shake gently at room temperature for 45 min. For other proteins, the optimal molar ratio may vary depending on protein structure and available reactive amine sites. For example, we use a 1:2 protein-to-tetrazine ratio for mesothelin.
40. Transfer the protein–tetrazine mixture to a freshly rinsed ultrafiltration column and wash the column five times with HEPES buffer to remove any unbound tetrazine. Discard the filtrate after each wash.
41. After the final wash, invert the column and centrifuge at 1,000g for 5 min to collect the antibody solution into a microcentrifuge tube.

#### ◆ TROUBLESHOOTING

42. Measure the final protein concentration again (as described in Step 38) to account for any loss during modification and purification. Then, add an equal volume of glycerol to the antibody or protein solution and mix thoroughly.  
■ **PAUSE POINT** Store the antibody preparation at –20 °C for up to 6 months.
43. On day 1 (fabrication Stage 3), transfer 3 million microbeads (referred to as a 3M synthetic cells batch) suspended in HEPES-CT into 2 mL microcentrifuge tubes for surface modification.
44. Centrifuge the microbeads at 6,000g for 5 min. Gently aspirate and discard the top 1.5 mL of the solution. Add 1.5 mL of MES-CT to the microcentrifuge tube.
45. Repeat Step 44. Then centrifuge the microbeads at 6,000g for 5 min. Gently aspirate and discard the top 1.5 mL of the solution.
46. Prepare conjugation A according to the formula in the table for the surface modification of a 3M microbead batch. Mix the prepared solution with the microbead pellets in the tube.

3M synthetic cells batch	Volume	Base buffer	EDC (mM)	NHS (mg/mL)
Conjugation A	0.5 mL	MES-CT	120	90

47. Seal the tube cap tightly with tape and place it on a roller for 1 h at room temperature.
48. Centrifuge the microbeads in a 2 mL microcentrifuge tube at 6,000g for 5 min. Gently aspirate and discard the top 1.5 mL of the supernatant. Add 1.5 mL of HEPES-CT to the tube.
49. Repeat Step 48. Centrifuge the microbead again at 6,000g for 5 min. Gently aspirate and discard the top 1.5 mL of the supernatant.
50. Add TCO-PEG4-amine dissolved in DMSO to the microbeads to achieve a final concentration of 4 mM. Allow the reaction to proceed overnight at room temperature in the dark.  
▲ **CRITICAL STEP** The TCO-PEG4-amine stock solution is prepared at 40 mM in DMSO and diluted tenfold to a final concentration of 4 mM in the reaction mixture. This results in a maximum final DMSO concentration of 10% (vol/vol), which does not affect downstream applications. Additionally, the subsequent dialysis step ensures complete removal of DMSO, preventing any residual cytotoxicity before cell culture use.
51. Transfer the solution to a 1,000 kDa dialysis bag. If the solution volume is less than 3 mL, add additional HEPES-CT to reach the required volume.
52. Dialyze the solution in 300 mL of HEPES-CT containing 0.02% sodium azide. Replace the dialysis buffer every 2 h for the first 8 h, then replace it every 12 h for the next 24 h.
53. On day 3 (fabrication Stage 3), collect the dialyzed solution from the dialysis bag. Rinse the dialysis bag with 2 mL of HEPES-CT containing 0.02% sodium azide and combine the rinse solution with the dialyzed solution.  
◆ **TROUBLESHOOTING**
54. Count the number of microbeads using a hemocytometer.

# Protocol

55. Add 6  $\mu\text{g}$  of purified antibody/protein–tetrazine complex (prepared in Step 42) per 3 million modified microbeads to the tube. Mix thoroughly and allow the reaction to proceed at room temperature for at least 4 h. For polyclonal T cell activation, anti-CD3 and anti-CD28 antibodies are mixed at a 1:1 ratio. For antigen-specific CART enrichment, mesothelin protein and anti-CD28 antibody are also mixed at a 1:1 ratio.

▲ **CRITICAL STEP** To ensure proper antibody conjugation, place the reaction tube on a roller mixer at ~10–15 rpm, allowing continuous gentle rotation. This prevents microbeads from settling while avoiding excessive shear forces that could disrupt surface interactions.

◆ **TROUBLESHOOTING**

## Fabrication Stage 4: storage

● **TIMING** 1 d

56. On day 0 (fabrication Stage 4), filter the microbead mixture through a 40  $\mu\text{m}$  cell strainer in a biosafety cabinet.
57. Transfer the filtered microbead mixture into 1.5 mL microcentrifuge tubes. Fill each tube to 1.5 mL with cell medium. Centrifuge at 6,000g for 5 min. Gently aspirate and discard the top 1.4 mL of the supernatant.
58. Add 1.4 mL of cell medium to the microcentrifuge tube. Centrifuge at 6,000g for 5 min. Gently aspirate and discard the top 1.4 mL of the supernatant.
59. Repeat Step 58 two more times, then vortex the microbead solution thoroughly. The synthetic cells are ready for use.
  - **PAUSE POINT** Store the synthetic cells at 4 °C for up to 2 months.

## T cell activation with synthetic cells

● **TIMING** 15 d

60. On day 0, thaw cryopreserved PBMCs quickly in a 37 °C water bath.
61. Transfer the thawed cells into a 15 mL conical tube containing 10 mL prewarmed complete lymphocyte culture medium.
62. Centrifuge the cells at 300g for 5 min at 4 °C.
63. Discard the supernatant.
64. Resuspend the cell pellet in a complete lymphocyte culture medium at a density of  $1 \times 10^6$  cells/mL.
65. Seed  $1 \times 10^6$  PBMCs into a 24-well plate.
  - ▲ **CRITICAL STEP** Plates are not fixed throughout the culture period. Depending on cell numbers postactivation, transition to 6-well plates, 10-cm tissue culture dishes or 15-cm tissue culture dishes as needed. Ensure that the cell concentration always remains below  $10^7$  cells/mL.
66. Add the synthetic cell suspension to PBMCs at a 1:1 cell number ratio in complete lymphocyte culture medium (that is, one synthetic cell per PBMC). Adjust the final volume to 1 mL per well or reaction by adding culture medium as needed. Mix gently and incubate under standard culture conditions.
  - ▲ **CRITICAL STEP** We have consistently used a default 1:1 ratio, and this ratio has not yet been optimized. However, it can be adjusted as needed to accommodate different experimental setups and requirements.
67. Mix thoroughly by gently pipetting up and down.
68. Supplement the complete lymphocyte culture medium containing PBMCs and synthetic cells with 30 ng/mL (~30,000 IU/ml) recombinant human IL-2. Mix gently and return the culture to the incubator under standard conditions (37 °C, 5% CO<sub>2</sub>) for continued stimulation.
69. On day 2, thaw concentrated lentivirus carrying the CAR gene. The virus generation and concentration methods have been described previously<sup>80,81</sup>.
70. Prepare the virus mixture by combining 20–40  $\mu\text{L}$  virus with 1:100 poloxamer syneronic F108 and 1:1,000 prostaglandin E2 (PGE2).
71. Add the mixture to the activated T cells.
72. Culture the transduced cells for another 24 h.

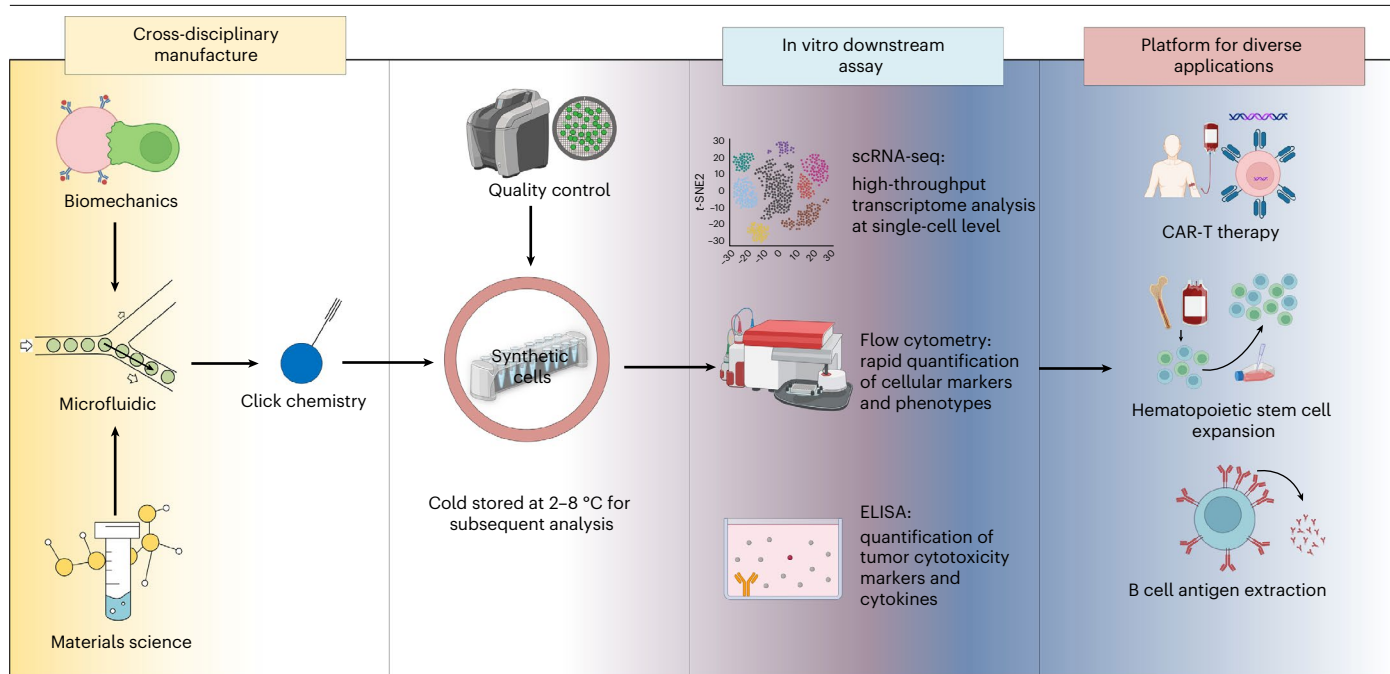


**Fig. 4 | Cross-disciplinary workflow for the development, manufacturing and application of synthetic cells.** The process integrates multiple scientific disciplines, including biomechanics, cell biology, microfluidics and materials science, to manufacture synthetic cells. Following cross-disciplinary production, synthetic cells undergo downstream assays such as scRNA-seq, flow cytometry,

ELISA and quality control analysis to ensure functionality. Synthetic cells serve as a versatile platform for diverse applications, including CAR-T therapy, hematopoietic stem cell expansion and B cell antigen extraction, highlighting their potential in basic research and translational medicine.

73. On day 3, add 500  $\mu\text{L}$  of fresh complete lymphocyte culture medium supplemented with 10 ng/mL of recombinant human IL-2.
  - ▲ **CRITICAL STEP** Keep the virus on ice during transduction, as room temperature will reduce the virus titer.
74. Culture the PBMC–synthetic cell mixture in a humidified incubator at 37 °C with 5%  $\text{CO}_2$  from day 3 to day 13.
75. Monitor cell density and viability daily.
  - ▲ **CRITICAL STEP** Donor-to-donor variations affect proliferation rates of the activated T cells. Daily monitoring is necessary to maintain a T cell density of  $0.5\text{--}1 \times 10^6$  cells/mL throughout the entire culture.
76. On day 13, if the activated T cells reach 70–80% confluency, collect the culture containing the activated T cells and the synthetic cells into a 15 mL or 50 mL conical tube. Centrifuge the cells at 300g for 5 min at 4 °C. Discard the supernatant. Resuspend the cell pellet in complete lymphocyte culture medium supplemented with 10 ng/mL recombinant human IL-2 at a cell density of  $0.5\text{--}1 \times 10^6$  cells/mL. Seed into appropriately sized tissue culture plates or dishes.
77. At day 14, determine CAR T cell expansion by counting the cells and calculating the fold expansion.
  - **PAUSE POINT** The synthetic cells activated CAR-T cells can be directly cryopreserved as the final therapeutic cell product.
  - ◆ **TROUBLESHOOTING**

## Downstream assays

### ● TIMING variable

78. After the successful expansion of CAR-T cells using synthetic cells, downstream assays can be performed to further characterize and evaluate their properties (Fig. 4). Building on

our previous comprehensive analyses, which assessed the functional capacity, phenotypic characteristics and gene expression profiles of CAR-T cells, we highlight key aspects relevant to this protocol.

To sample the mechanical properties of synthetic cells to validate their viscoelastic behavior, follow option A.

● **TIMING** ~1 d

To quantify antibody density on synthetic cells, follow option B.

● **TIMING** ~1 d

For SEM-based analyses to examine physical interactions between T cells and synthetic cells and to visualize immunological synapse formation, follow option C.

● **TIMING** ~1–2 d

For flow cytometry-based evaluations of key cell surface markers such as CD8 and CD69 to determine activation and memory potential, follow option D.

● **TIMING** ~4–6 h

For scRNA-seq to uncover detailed functional and genetic profiles of CAR-T cell subpopulations, follow option E.

● **TIMING** ~2–3 d excluding sequencing time

To perform an in vitro tumor cell killing assay, follow option F.

● **TIMING** 1–3 d depending on experimental setup

(A) **Mechanical property measurement of synthetic cells and native APCs**

- (i) For synthetic cell measurement, use antibody-conjugated beads (V1, V2, E1 or E2) prepared as described above in the Procedure. To enable fluorescence-based visualization under AFM, label the beads by incubating them with a fluorescently tagged secondary antibody specific to the conjugated primary antibody (for example, anti-CD3 or anti-CD28). In addition, bare beads conjugated with GFP via EDC/NHS chemistry can be used as a control group to verify that antibody conjugation does not alter the intrinsic mechanical properties of the microbeads. The conjugation method for GFP has been described in our previous study<sup>82</sup> (using microbeads obtained from Step 34).  
▲ **CRITICAL STEP** Fluorescent labeling is recommended to facilitate localization of microbeads during AFM imaging as the hydrogel beads may appear optically transparent under bright-field microscopy. However, if the beads can be clearly identified without fluorescence, this step is optional.
- (ii) For native APCs measurement, collect differentiated APCs from the culture medium. To also enable positional identification of APCs under AFM-fluorescence imaging, stain the cells with Hoechst dye using standard protocols if needed.
- (iii) Place a small aliquot of the equilibrated sample, including either antibody-conjugated beads or native APCs, onto a polylysine-treated clean glass-bottom confocal dish. Allow the sample to settle for a few minutes.
- (iv) Mount the sample dish onto the stage of an AFM. A bio-AFM system with a separate AFM head is recommended as it allows simultaneous optical microscopy without interfering with fluorescence imaging (Fig. 3b).
- (v) Perform force spectroscopy on individual samples, including synthetic cells (V1, V2), elastic beads (E1, E2) and native APCs. Once the force setpoint (for example, 10 nN) is reached during the extension phase, hold the AFM tip at a constant height for a specified duration (for example, 30 s) to measure stress relaxation (monitoring vertical deflection force changes over time; Fig. 3c,d).
- (vi) Use the Hertz model to calculate Young's modulus from the obtained force curves (Fig. 3e). JPK data processing can be used to fit curves and determine modulus.  
▲ **CRITICAL STEP** Accurate modulus determination using the Hertz model relies on the following key assumptions: the AFM probe must have a spherical tip, the material/cell surface should exhibit low curvature relative to the tip, deformations must remain small and the sample must be sufficiently thick relative to the indentation to prevent substrate boundary effects. To meet these conditions, a cylindrical-tipped AFM probe with an appropriate spring constant (~0.25 N/m)

and radius (~1  $\mu\text{m}$ ) is required. For higher precision, a precalibrated cantilever with laser Doppler velocimetry is preferred. Above all, the Bruker SAA-SPH-1UM probe is recommended.

- (vii) Compare the mechanical properties of synthetic cells (V1, V2), elastic beads (E1, E2) and native APCs based on the measured Young's modulus and stress-relaxation data. The same AFM-based procedure described above is used for both sample types to ensure comparability.
  - (viii) (Optional) As an alternative or complementary approach, the mechanical properties of different formulations (V1, V2, E1, E2) can also be measured using bulk gel techniques such as uniaxial compression testing or rheometry. These methods provide independent validation of Young's modulus and stress-relaxation behavior observed in AFM-based single-bead assays. Detailed protocols for these bulk mechanical measurements can be found in previous publications<sup>27,83</sup>.
- (B) **Quantification of antibody density on synthetic cells**
- ▲ **CRITICAL** To ensure the accurate measurement of surface antibody density, a dedicated batch of fluorescently labeled synthetic cells should be prepared separately from the standard experimental batch. This batch should be modified using FITC-conjugated anti-CD3, rather than the standard anti-CD3/anti-CD28 mixture, to allow for direct fluorescence-based quantification.
- (i) Prepare a separate batch of  $1 \times 10^6$  synthetic cells.
  - (ii) Modify these synthetic cells with anti-CD3 FITC using the click chemistry methods outlined above (Step 36), instead of the standard anti-CD3/anti-CD28 conjugation.
  - (iii) Wash the synthetic cells twice in HEPES-CT buffer to remove unbound antibody.
  - (iv) Resuspend the cells in 500  $\mu\text{L}$  of HEPES-CT buffer for analysis.
  - (v) Perform flow cytometry to measure fluorescence intensity.
  - (vi) Construct a standard calibration curve using Quantum Simply Cellular anti-Mouse IgG beads (Bang Laboratories, 815) stained with anti-CD3 FITC.
  - (vii) Quantify the average antibody density per synthetic cell based on the fluorescence signal and standard curve.
- (C) **SEM-based analysis of T cell–synthetic cells interactions**
- (i) Coculture  $1 \times 10^6$  T cells with synthetic cells in a 24-well plate for 24 h.
  - (ii) Prepare 0.1 M Sorensen's phosphate buffer (pH 7.2) with 0.025 M of  $\text{NaH}_2\text{PO}_4 \cdot \text{H}_2\text{O}$  and 0.075 M of  $\text{NaHPO}_4 \cdot 7\text{H}_2\text{O}$ .
  - (iii) Cut a silicon wafer square to fit in both the critical point dryer container and the bottom of a single well in a 24-well plate. Coat it with poly-L-lysine and put it at the bottom of a well.
  - (iv) Gently aspirate the cell–bead mixture and pipette toward the silicon wafer. Centrifuge the plate at 300g for 5 min.
  - (v) Remove the cell medium and rinse the cells with 0.1 M Sorensen's phosphate buffer (pH 7.2) for 30 s. Remove the buffer.
  - (vi) Fix cocultured samples with 2.5% paraformaldehyde (diluted with Sorensen's phosphate buffer) for 30 min at room temperature in a fume hood.
  - (vii) Rinse the fixed specimens in Sorensen's phosphate buffer 3 times, 10 min each rinse.
  - (viii) Fix in 1% osmium tetroxide in the fume hood for 30 min.
  - (ix) Rinse with Sorensen's phosphate buffer 3 times (10 min each rinse).
  - (x) Dehydrate the samples using a graded ethanol series (70%, 80%, 90%) for 10 min per step. Then dehydrate in 95% and finally in 100% alcohol (2 changes each; 10 min for each one).
  - (xi) Critical-point dry the samples.
  - (xii) Coat samples with a ~5 nm gold layer using a sputter coater.
  - (xiii) Image the samples under a scanning electron microscope (SEM) to visualize immunological synapse formation and bead–cell interactions.

◆ **TROUBLESHOOTING**

**Table 6 | Comprehensive antibodies for phenotyping human T cell function**

Antibody	Target marker	Cell subset	Function/significance
Anti-CD3	CD3	T cells (pan marker)	General T cell marker for identifying all T cell populations
Anti-CD4	CD4	Helper T cells	Identifies CD4 <sup>+</sup> T helper cells
Anti-CD8	CD8	Cytotoxic T cells	Identifies CD8 <sup>+</sup> cytotoxic T cells
Anti-CCR7	CCR7	Naive and central memory T cells	Involved in T cell homing to lymphoid tissues and indicates memory status
Anti-CD45RA	CD45RA	Naive T cells	Marker of naive T cells, often used with CCR7 for differentiation stages
Anti-CD95 (FAS)	CD95	TMSCs	High expression in TMSCs, associated with self-renewal capability
Anti-CD62L (SELL)	CD62L	Naive and central memory T cells	Important for T cell homing; high in TMSCs and central memory T cells
Anti-CD45RO	CD45RO	Memory T cells	Indicates memory phenotype, typically higher in effector memory T cells
Anti-CD122 (IL2R $\beta$ )	IL2R $\beta$	TMSCs	Associated with T cell survival and homeostatic proliferation in TMSCs
Anti-TCF7	TCF7	TMSCs	Transcription factor promoting T cell stemness
Anti-LEF1	LEF1	TMSCs	Works with TCF7 in maintaining stemness and multipotency of TMSCs
Anti-CD69	CD69	Activated T cells	Early activation marker, helps assess T cell activation status
Anti-PD-1	PD-1	Exhausted T cells	Marker of T cell exhaustion, often used to assess functional decline
Anti-LAG3	LAG3	Exhausted T cells	Co-inhibitory receptor linked to T cell exhaustion
Anti-TIM-3	TIM-3	Exhausted T cells	Marker for exhaustion, involved in immune checkpoint regulation
Anti-Ki67	Ki67	Proliferating T cells	Indicates active proliferation and cell cycle progression
Anti-CXCR3	CXCR3	Effector and memory T cells	Associated with migration to inflamed tissues and memory function
Anti-GZMB	Granzyme B	Cytotoxic T cells	Marker of cytolytic function, involved in inducing target cell apoptosis
Anti-PRF1	Perforin	Cytotoxic T cells	Facilitates the entry of granzyme into target cells

**Table 7 | Comprehensive antibodies for phenotyping mouse T cell function**

Antibody	Target marker	Cell subset	Function/significance
Anti-CD3	CD3 <sup>+</sup>	Naive T cells	Important for T cell activation and signal transduction
Anti-CD4	CD4 <sup>+</sup>	Effector CD4 <sup>+</sup> T cells	Coordinating the immune system's reaction to pathogens and other foreign invaders
Anti-CD8	CD8 <sup>+</sup>	Effector CD8 <sup>+</sup> T cells	Play a crucial role in adaptive immune response to viral infections, tumors and other abnormal cells
Anti-CD8	CD8 <sup>-</sup>	CD4 <sup>+</sup> T cells	Recognizing and killing infected or cancerous cells
Anti-CD44	CD44 <sup>+</sup>	Effector CD44 <sup>+</sup> T Cells	Cell adhesion, migration and signaling
Anti-CCR7	CCR7 <sup>+</sup>	Naive T cells and central memory t cells	Migration and homing of T cells to secondary lymphoid organs
Anti-CD45RB <sup>hi</sup>	CD45RB <sup>hi</sup>	Naive T cells	Regulating T cell signaling
Anti-CD45RB <sup>lo</sup>	CD45RB <sup>lo</sup>	Effector T cells	Signaling and activation
Anti-CD62L	CD62L <sup>+</sup>	Naive T cells and effector memory T cells	Trafficking and migration of various immune cells
Anti-CD45RO	CD45RO <sup>+</sup>	Memory T cells	Activation and differentiation of T cells
Anti-PD-1	PD-1	Exhausted T cells	Regulating immune responses, particularly in the context of immune checkpoints
Anti-LAG3	LAG3	Exhausted T cells	Regulating immune responses, particularly in immune tolerance, T cell activation and exhaustion
Anti-Tim-3	Tim-3	Exhausted T cells	Regulating T cell responses and maintaining immune homeostasis
Anti-CXCR5	CXCR5	T follicular helper cells	Migration and positioning of immune cells
Anti-GZMB	Granzyme B	Cytotoxic T cells	Inducing target cell death as part of the immune response against infected cells, tumors and foreign pathogens
Anti-PRF1	Perforin	Cytotoxic T cells	Functioning as key effector molecule in cell-mediated cytotoxicity

**(D) Cell surface marker analysis**

- (i) Collect CAR-T cells from the culture setup at timepoints of interest (Steps 60–77) and wash them twice with PBS containing 1% FBS.
- (ii) Resuspend  $1 \times 10^6$  cells in 100  $\mu$ L of staining buffer.

# Protocol

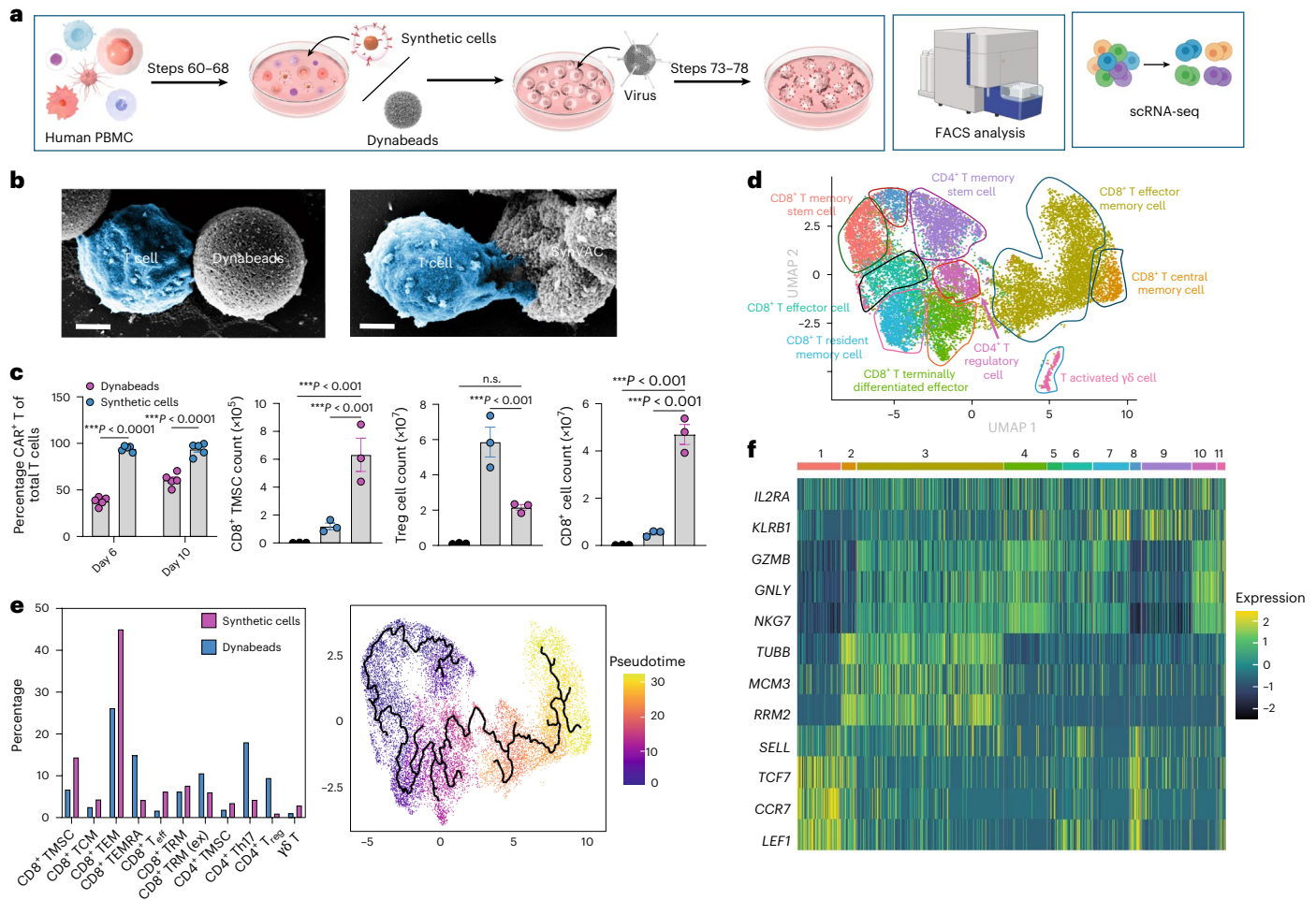


**Fig. 5 | Comparison of CAR-T cell expansion and characterization using synthetic cells versus Dynabeads. a**, A schematic illustration of the workflow for CAR-T cell expansion, FACS analysis and scRNA-seq. Human PBMCs are activated and expanded using synthetic cells or Dynabeads, followed by virus transduction to generate CAR-T cells for downstream analysis. **b**, SEM images showing physical interactions between T cells and Dynabeads (left) or synthetic cells (right). Scale bars, 2  $\mu\text{m}$ . **c**, Quantitative analysis of CAR-T expansion and T cell subsets. CAR-T cell percentages at day 6 and day 10 ( $n = 6$ ), total CD8<sup>+</sup> TMSC counts, T<sub>reg</sub> cell counts and CD8<sup>+</sup> T cell counts are compared between synthetic cells and Dynabeads at day 14 ( $n = 3$ ). Data are shown as the mean  $\pm$  s.e.m. Statistical significance: \*\*\* $P < 0.001$ . **d**, A Uniform Manifold Approximation and Projection (UMAP) plot of scRNA-seq analysis showing distinct T cell

subpopulations, including CD8<sup>+</sup> TMS, central memory cells, effector memory cells and other T cell subsets. **e**, Quantification of T cell subsets expanded using synthetic cells versus Dynabeads, showing a higher proportion of CD8<sup>+</sup> TMSs and reduced T<sub>reg</sub> cells in the synthetic cell group. Pseudotime analysis highlights T cell differentiation trajectories. TCM, central memory T cells; TEM, effector memory T cells; TEMRA, terminally differentiated effector memory RA T cells; T<sub>eff</sub>, effector T cells; TRM, resident memory T cells; TRM (ex), exhausted resident memory T cells; Th17, T helper 17 cells;  $\gamma\delta$  T,  $\gamma\delta$  T cells. **f**, A heat map of gene expression profiles across T cell subsets, showing differential expression of key genes (for example, *IL2RA*, *KLRB1*, *SELL*, *LEF1*, *TCF7*) associated with T cell activation, memory and stemness. Panels **b**–**f** adapted from ref. 27, Springer Nature Limited.

- (iii) For CAR-T cell phenotype analysis, add fluorescently labelled antibodies (for example, CD4, CD8, CD69, CCR7 and CD45RO) to the cell suspension and incubate on ice in the dark for 30 min (Tables 6 and 7). For CAR-T cell CAR transduction analysis, stain the activated CAR-T cells with goat anti-mouse IgG F(ab')<sub>2</sub> secondary antibody (ThermoFisher, 31803) at a 1:50 dilution and perform a second staining step using fluorescence-conjugated streptavidin antibody (Biolegend, 405207) at a 1:1,000 dilution.

▲ **CRITICAL STEP** Include PBMC-derived T cells without CAR engineering as a staining control to determine the CAR transduction rate.

- (iv) Wash the cells twice with PBS and resuspend them in 200  $\mu\text{L}$  of PBS for analysis.

**Table 8 | Gene markers for identifying T cell functional states, exhaustion, and stemness based on single-cell sequencing**

T cell state	Markers	Description	Refs.
Functional	IFNG, TNF, GZMB, PRF1	Cytotoxicity and activation in response to antigens	91,92
Proliferative	MKI67, PCNA	Indicates active cell division and proliferation	93,94
Exhausted	PDCD1 (PD-1), LAG3, TIGIT, HAVCR2 (TIM-3)	Markers of T cell exhaustion, reduced effector function	95,96
Memory	CCR7, SELL (CD62L), IL7R	Associated with memory T cells and long-term immunity	97
Stemness (TMSCs)	TCF7, LEF1, CD95 (FAS), IL2R $\beta$ (CD122)	Self-renewal capacity, multipotency, long-term persistence	98,99
Effector Memory	GZMK, GZMH, CX3CR1	Associated with effector memory T cells	100
Naive	TCF7, CCR7, CD45RA	Characteristics of naive T cells, precursor of other T cell subsets	101

(v) Analyze the stained cells using flow cytometry, ensuring at least 10,000 events are collected per sample (Fig. 5a–c).

**(E) scRNA-seq**

- (i) Collect CAR-T cells from the cell culture, count cell number and access cell viability.
- (ii) FACS sort live CAR-T cells using Fixable Viability Dye eFluor506 (e506; eBioscience, 65-0866-14) and anti-human CD3 antibody (BioLegend, 300330). Collect the sorted cells in sterile collection tubes.
- (iii) Resuspend the sorted CAR-T cells in 1 $\times$  PBS with 0.04% BSA solution. The ideal concentration for single cell capture is 700–1,200 cells/ $\mu$ L in 100  $\mu$ L volume to target 10,000 cells (or 1,300–1,600 cells/ $\mu$ L to target 20,000 cells).

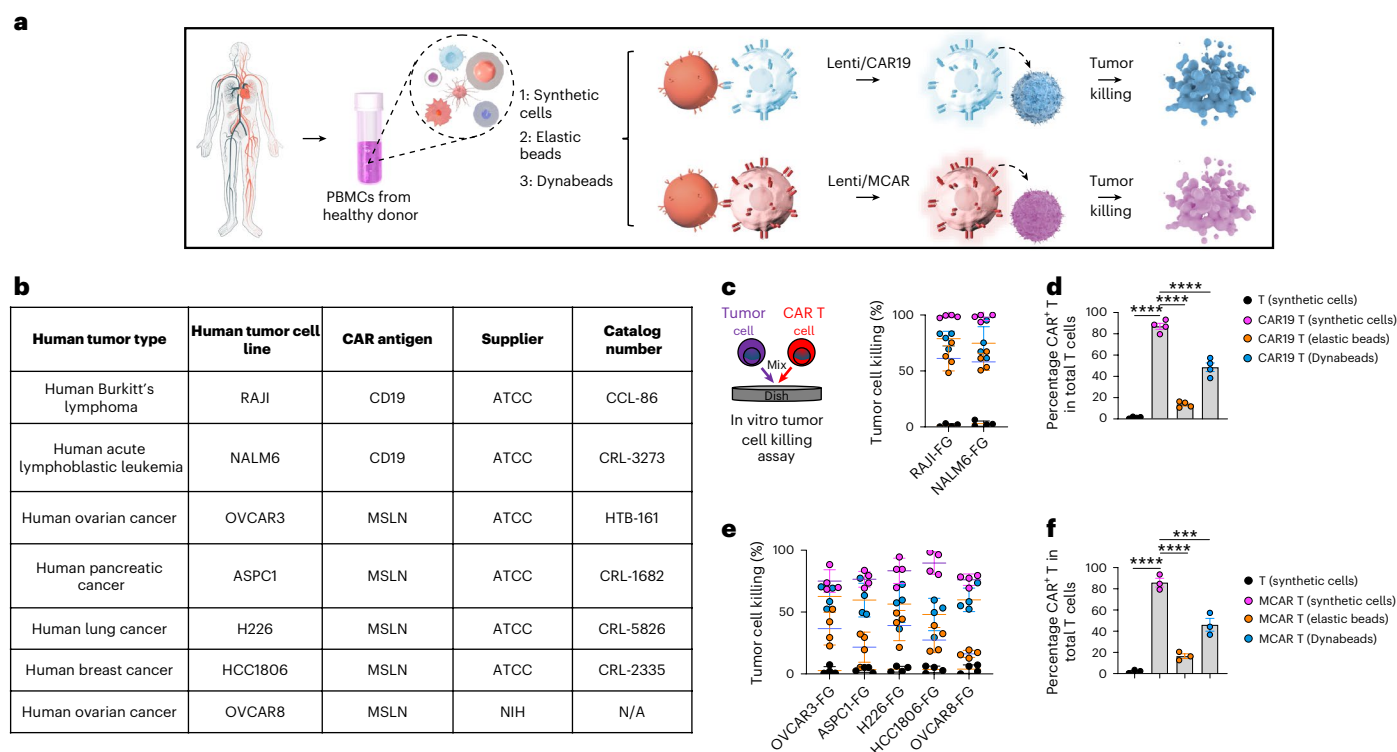


**Fig. 6 | CAR-T cell expansion and tumor-killing efficacy using synthetic cells, elastic beads and Dynabeads. a**, A schematic illustration of the workflow for CAR-T cell expansion using different activation platforms (synthetic cells V1, elastic beads E1 and Dynabeads) and their tumor-killing activity. **b**, A table listing the human tumor cell lines, CAR antigens, suppliers and catalog numbers used for in vitro tumor-killing assays. **c**, A diagram of the in vitro tumor-killing assay setup (left) and quantification of tumor cell killing by CAR19 T cells against RAJI (Burkitt's lymphoma) and NALM6 (acute lymphoblastic leukemia) cell lines

(right) ( $n = 4$ ). FG indicates cell lines expressing firefly luciferase and enhanced GFP. **d**, The percentage of CAR19<sup>+</sup> T cells in total T cells expanded using synthetic cells, elastic beads or Dynabeads ( $n = 4$ ). **e**, Quantification of tumor cell killing by CAR-T cells targeting mesothelin (MSLN) across multiple tumor cell lines, including OVCAR3, ASPC1, H226, HCC1806 and OVCAR8 cell lines ( $n = 4$ ). **f**, The percentage of MCAR<sup>+</sup> T cells in total T cells expanded using synthetic cells, elastic beads or Dynabeads ( $n = 3$ ). Data are shown as the mean  $\pm$  s.e.m. Statistical significance is indicated: \*\*\* $P < 0.001$ , \*\*\*\* $P < 0.0001$ .

# Protocol

(iv) Perform scRNA-seq and the subsequent analyses (Fig. 5d–f and Table 8).

▲ **CRITICAL STEP** Commercial platforms, such as 10X Genomics, may be utilized for these procedures. In our supporting study<sup>27</sup>, all scRNA-seq experiments were conducted at the UCLA Technology Center for Genomics and Bioinformatics (TCGB) core facility.

**(F) Tumor cell killing assay**

- (i) Plate target tumor cells (for example,  $1 \times 10^5$  RAJI or OVCAR3 cells per well) in a 96-well plate and allow them to adhere or equilibrate overnight.
- (ii) Collect CAR-T cells and adjust the concentration to achieve desired effector-to-target (E:T) ratios (for example, 1:1, 2:1, 5:1, 10:1).
- (iii) Add CAR-T cells to tumor cells in duplicate wells for each condition and incubate at 37 °C with 5% CO<sub>2</sub> for 24–48 h.
- (iv) Collect the coculture supernatants for cytokine analysis (for example, IFN- $\gamma$  and TNF) and collect cells for viability assays.
- (v) Stain cells with a viability dye (for example, 7-AAD or e506) and analyze tumor cell death using flow cytometry. Live tumor cells are identified as e506<sup>-</sup>GFP<sup>+</sup> cells.
- (vi) Record and compare cytotoxicity across different E:T ratios to assess CAR-T cell killing efficiency (Fig. 6).

## Troubleshooting

Troubleshooting advice can be found in Table 9.

**Table 9 | Troubleshooting table**

Steps	Problem	Possible reason	Solution
7	Deformation of SU-8 structures	Incorrect exposure time	Test gradient exposures
		Poor wafer–photomask contact	Verify exposure system supports VAC mode
17	SU-8 detaches during PDMS peeling	Prolonged wafer storage or surface contamination reduces adhesion	Use fresh wafers; clean with pressurized nitrogen before spin-coating SU-8
22	Bonding failure	Glass slide and PDMS surfaces are not clean	Extend and repeat cleaning steps in Step 19; avoid surface contact after cleaning
24	No microspheres; phase separation	Plasma treatment made surfaces too hydrophilic	Reduce plasma time
			Leave bonded device unused for a week before experiments
34	Microspheres unstable; not collected	Viscosity mismatch between alginate and oil phases causes turbulence	Use specified alginate/CMC products Adjust CMC concentration; use Reynolds number as a guide
41	Low antibody recovery	Buffers may not be freshly prepared or at the correct pH	Verify centrifugation steps
			Use fresh pH-adjusted buffers
			Ensure column does not bind antibodies
53	Low microsphere number after dialysis	Possible leaking during EDC/NHS reaction Not enough solution in the dialysis bag	Make sure the cap is closed tightly during EDC/NHS reaction
			Add more buffer to the dialysis bag at the beginning of dialysis
			Ensure the microspheres are fresh
55	Low ligand density after click reaction	Possible hydrolysis of the activated carboxylate group	Ensure the pH of buffers are correct
			Ensure the microspheres are fresh
			Ensure that microspheres are washed into HEPES buffer as soon as possible
77	T cells growing slow	Sodium azide in the microsphere's solution may not be removed fully	Centrifuge for an additional time when washing the microspheres into cell culture medium
78(C)(xiii)	Cells look deformed under SEM	Critical point drying may not be done correctly	Strictly follow manufacturer protocol
			Increase the time of each gradient alcohol
78(C)(xiii)	Cells look unclear under SEM	Gold layer may not be thick enough	Increase the time of gold sputtering
			Decrease the voltage of the SEM

---

## Timing

---

Steps 1–26, Fabrication Stage 1 (manufacture of device and microbeads): 5 d  
Steps 27–34, Fabrication Stage 2 (processing of microbeads): 1–2 d  
Steps 35–55, Fabrication Stage 3 (surface chemistry): 4 d  
Steps 56–59, Fabrication Stage 4 (storage): 1 d  
Steps 60–77, T cell activation with synthetic cells: 15 d  
Steps 78, Downstream assays  
Option A (AFM measurement of synthetic cells or APCs): -1 d  
Option B (ligand density quantification): -1 d  
Option C (SEM imaging of immune synapse): -1–2 d  
Option D (flow cytometry for activation/memory markers): ~4–6 h  
Option E (scRNA-seq): ~2–3 d (excluding sequencing time)  
Option F (tumor cell killing assay): 1–3 d (depending on experimental setup)

---

## Anticipated results

We have shown in previous work that synthetic cells provide superior activation and expansion of CAR-T cells compared with Dynabeads<sup>27</sup>. Human PBMCs activated with synthetic cells undergo robust expansion to generate CAR-T cells, followed by flow cytometry and scRNA-seq analysis (Fig. 5a). SEM images show that T cells exhibit more extensive interactions with synthetic cells than Dynabeads, suggesting enhanced activation (Fig. 5b). Quantitative analysis confirms that CAR-T cells expanded using synthetic cells achieve notably higher transduction efficiency, with a greater proportion of CAR-expressing T cells by day 10 ( $P < 0.001$ ). Additionally, the total number of CD8<sup>+</sup> TMSCs is markedly increased, reflecting an improved capacity for generating long-lasting immune responses. CD8<sup>+</sup> T cell expansion is also higher, promoting a more cytotoxic T cell phenotype, while the population of CD4<sup>+</sup> T<sub>reg</sub> cells decreases, ensuring that immunosuppressive effects are reduced (Fig. 5c). scRNA-seq analysis further reveals distinct T cell subset distributions. Synthetic cells generate a higher fraction of CD8<sup>+</sup> memory and effector T cells (Fig. 5d), whereas Dynabeads result in a larger proportion of terminally differentiated T cells<sup>27</sup>. This trend is confirmed by quantification of T cell subsets, showing that synthetic cells preferentially expand CD8<sup>+</sup> TMSCs while reducing T<sub>reg</sub> cells (Fig. 5e). At the gene expression level, synthetic cell-expanded T cells upregulate key markers associated with T cell activation, stemness, and persistence, such as *IL2RA*, *LEF1*, *TCF7* and *SELL* (Fig. 5f). These enhancements in CAR-T cell expansion and memory formation translate into superior functional performance (Table 8).

CAR-T cells expanded using synthetic cells exhibit higher tumor cell killing potency than those expanded using Elastic beads or Dynabeads (Fig. 6). Cytotoxicity assays show that CAR19 T cells efficiently eliminate RAJI (Burkitt's lymphoma) and NALM6 (acute lymphoblastic leukemia) cells, achieving higher killing percentages than Dynabeads-expanded cells (Fig. 6c). A similar trend is observed across multiple cancer types expressing mesothelin (MSLN), including ovarian (OVCAR3, OVCAR8), pancreatic (ASPC1), lung (H226) and breast (HCC1806) cancers, where CAR-T cells expanded using synthetic cells consistently demonstrate superior tumor-killing efficiency (Fig. 6e). The percentage of CAR19<sup>+</sup> and mesothelin-targeting CAR (MCAR)<sup>+</sup> T cells is also higher in the synthetic cell-expanded groups compared with Elastic bead and Dynabead groups, reinforcing the advantage of synthetic cells in generating highly functional CAR-T cells (Fig. 6d,f). Together, these results highlight the clinical potential of using synthetic cells to optimize CAR-T therapy in both hematologic malignancies and solid tumors.

## Reporting summary

Further information on research design is available in the Nature Portfolio Reporting Summary linked to this article.

## Data availability

The genomics (scRNA-seq) data were obtained from the public repository Gene Expression Omnibus (GEO) database (accession code [GSE242531](#); related to Fig. 5d–f). Additional information and materials will be made available upon reasonable request. Source data are provided with this paper.

Received: 12 November 2024; Accepted: 8 August 2025;

Published online: 09 October 2025

## References

1. Ying, Z. et al. A safe and potent anti-CD19 CAR T cell therapy. *Nat. Med.* **25**, 947–953 (2019).
2. Faruqi, A. J. et al. The impact of race, ethnicity, and obesity on CAR T-cell therapy outcomes. *Blood Adv.* **6**, 6040–6050 (2022).
3. Liu, Y., Sperling, A. S., Smith, E. L. & Mooney, D. J. Optimizing the manufacturing and antitumour response of CAR T therapy. *Nat. Rev. Bioeng.* **1**, 271–285 (2023).
4. Baker, D. J., Arany, Z., Baur, J. A., Epstein, J. A. & June, C. H. CAR T therapy beyond cancer: the evolution of a living drug. *Nature* **619**, 707–715 (2023).
5. Vormittag, P., Gunn, R., Ghorashian, S. & Veraitch, F. S. A guide to manufacturing CAR T cell therapies. *Curr. Opin. Biotechnol.* **53**, 164–181 (2018).
6. Thauland, T. J., Hu, K. H., Bruce, M. A. & Butte, M. J. Cytoskeletal adaptivity regulates T cell receptor signaling. *Sci. Signal.* **10**, eaah3737 (2017).
7. Shah, K., Al-Haidari, A., Sun, J. & Kazi, J. U. T cell receptor (TCR) signaling in health and disease. *Signal Transduct. Target. Ther.* **6**, 412 (2021).
8. Seaman, K., Sun, Y. & You, L. Recent advances in cancer-on-a-chip tissue models to dissect the tumour microenvironment. *Med-X* **11**, 11 (2023).
9. Cheung, A. S., Zhang, D. K. Y., Koshy, S. T. & Mooney, D. J. Scaffolds that mimic antigen-presenting cells enable ex vivo expansion of primary T cells. *Nat. Biotechnol.* **36**, 160–169 (2018).
10. Hernandez-Lopez, R. A. et al. T cell circuits that sense antigen density with an ultrasensitive threshold. *Science* **371**, 1166–1171 (2021).
11. Chen, W. & Zhu, C. Mechanical regulation of T-cell functions. *Immunol. Rev.* **256**, 160–176 (2013).
12. Hu, K. H. & Butte, M. J. T cell activation requires force generation. *J. Cell Biol.* **213**, 535–542 (2016).
13. Kaech, S. M., Wherry, E. J. & Ahmed, R. Effector and memory T-cell differentiation: implications for vaccine development. *Nat. Rev. Immunol.* **2**, 251–262 (2002).
14. Valpione, S. et al. The T cell receptor repertoire of tumor infiltrating T cells is predictive and prognostic for cancer survival. *Nat. Commun.* **12**, 4098 (2021).
15. Wong, S. H. D. et al. Mechanical manipulation of cancer cell tumorigenicity via heat shock protein signaling. *Sci. Adv.* **9**, eadg9593 (2023).
16. Moulton, V. R. & Farber, D. L. Committed to memory: lineage choices for activated T cells. *Trends Immunol.* **27**, 261–267 (2006).
17. Zhang, J. et al. Osr2 functions as a biomechanical checkpoint to aggravate CD8<sup>+</sup> T cell exhaustion in tumor. *Cell* **187**, 3409–3426 (2024).
18. Ukrainskaya, V. et al. Antigen-specific stimulation and expansion of CAR T cells using membrane vesicles as target cell surrogates. *Small* **17**, e2102643 (2021).
19. Zhang, D. K. Y., Cheung, A. S. & Mooney, D. J. Activation and expansion of human T cells using artificial antigen-presenting cell scaffolds. *Nat. Protoc.* **15**, 773–798 (2020).
20. Agarwalla, P. et al. Bioinspired implantable scaffolds for rapid in vivo manufacture and release of CAR-T cells. *Nat. Biotechnol.* **40**, 1250–1258 (2022).
21. Hickey, J. W. et al. Engineering an artificial T-cell stimulating matrix for immunotherapy. *Adv. Mater.* **31**, e1807359 (2019).
22. Majedi, F. S. et al. Cytokine secreting microparticles engineer the fate and the effector functions of T cells. *Adv. Mater.* **30**, 1703178 (2018).
23. Majedi, F. S. et al. T-cell activation is modulated by the 3D mechanical microenvironment. *Biomaterials* **252**, 120058 (2020).
24. Tao, Y., Ju, E., Ren, J. & Qu, X. Immunostimulatory oligonucleotides-loaded cationic graphene oxide with photothermally enhanced immunogenicity for photothermal/immune cancer therapy. *Biomaterials* **35**, 9963–9971 (2014).
25. Deng, B. et al. Different T-cell activation approaches impact the resulting CART-cell products and possible clinical outcomes. *Blood* **144**, 4856–4856 (2024).
26. Eggermont, L. J., Paulis, L. E., Tel, J. & Figdor, C. G. Towards efficient cancer immunotherapy: advances in developing artificial antigen-presenting cells. *Trends Biotechnol.* **32**, 456–465 (2014).
27. Liu, Z. et al. Viscoelastic synthetic antigen-presenting cells for augmenting the potency of cancer therapies. *Nat. Biomed. Eng.* **8**, 1615–1633 (2024).
28. Labanieh, L. & Mackall, C. L. CAR immune cells: design principles, resistance and the next generation. *Nature* **614**, 635–648 (2023).
29. Cieri, N. et al. IL-7 and IL-15 instruct the generation of human memory stem T cells from naive precursors. *Blood* **121**, 573–584 (2013).
30. Gattinoni, L., Speiser, D. E., Lichterfeld, M. & Bonini, C. T memory stem cells in health and disease. *Nat. Med.* **23**, 18–27 (2017).
31. Dustin, M. L. The immunological synapse. *Cancer Immunol. Res.* **2**, 1023–1033 (2014).
32. Jin, W. et al. T cell activation and immune synapse organization respond to the microscale mechanics of structured surfaces. *Proc. Natl Acad. Sci. USA* **116**, 19835–19840 (2019).
33. Kummerow, C. et al. The immunological synapse controls local and global calcium signals in T lymphocytes. *Immunol. Rev.* **231**, 132–147 (2009).
34. Saththaporn, S. et al. Dendritic cells are dysfunctional in patients with operable breast cancer. *Cancer Immunol. Immunother.* **53**, 510–518 (2004).
35. Shinde, P., Fernandes, S., Melinkeri, S., Kale, V. & Limaye, L. Compromised functionality of monocyte-derived dendritic cells in multiple myeloma patients may limit their use in cancer immunotherapy. *Sci. Rep.* **8**, 5705 (2018).
36. Wolf, M. & Greenberg, P. D. Antigen-specific activation and cytokine-facilitated expansion of naive, human CD8<sup>+</sup> T cells. *Nat. Protoc.* **9**, 950–966 (2014).
37. Deniger, D. C. et al. Activating and propagating polyclonal gamma delta T cells with broad specificity for malignancies. *Clin. Cancer Res.* **20**, 5708–5719 (2014).
38. Xu, J., Melenhorst, J. J. & Fraietta, J. A. Toward precision manufacturing of immunogene T-cell therapies. *Cytotherapy* **20**, 623–638 (2018).
39. Suhoski, M. M. et al. Engineering artificial antigen-presenting cells to express a diverse array of co-stimulatory molecules. *Mol. Ther.* **15**, 981–988 (2007).
40. Li, Y. & Kurlander, R. J. Comparison of anti-CD3 and anti-CD28-coated beads with soluble anti-CD3 for expanding human T cells: differing impact on CD8 T cell phenotype and responsiveness to restimulation. *J. Transl. Med.* **8**, 104 (2010).
41. Al-Aghbar, M. A., Jainarayanan, A. K., Dustin, M. L. & Roffler, S. R. The interplay between membrane topology and mechanical forces in regulating T cell receptor activity. *Commun. Biol.* **5**, 40 (2022).
42. Yuan, D. J., Shi, L. & Kam, L. C. Biphasic response of T cell activation to substrate stiffness. *Biomaterials* **273**, 120797 (2021).
43. Zhu, E. et al. Biomimetic cell stimulation with a graphene oxide antigen-presenting platform for developing T cell-based therapies. *Nat. Nanotechnol.* **19**, 1914–1922 (2024).
44. Mock, U. et al. Automated manufacturing of chimeric antigen receptor T cells for adoptive immunotherapy using CliniMACS prodigy. *Cytotherapy* **18**, 1002–1011 (2016).
45. Abou-el-Nein, M. et al. Scalable manufacturing of CAR T cells for cancer immunotherapy. *Blood Cancer Discov.* **2**, 408–422 (2021).
46. Trickett, A. & Kwan, Y. L. T cell stimulation and expansion using anti-CD3/CD28 beads. *J. Immunol. Methods* **275**, 251–255 (2003).
47. Delcassian, D., Sattler, S. & Dunlop, I. E. T cell immunoengineering with advanced biomaterials. *Integr. Biol.* **9**, 211–222 (2017).
48. Li, A. W. et al. Engineering potent chimeric antigen receptor T cells by programming signaling during T-cell activation. *Sci. Rep.* **14**, 21331 (2024).
49. Agarwal, P. et al. One-step microfluidic generation of pre-hatching embryo-like core-shell microcapsules for miniaturized 3D culture of pluripotent stem cells. *Lab Chip* **13**, 4525–4533 (2013).
50. Chung, B. G., Lee, K.-H., Khademhosseini, A. & Lee, S.-H. Microfluidic fabrication of microengineered hydrogels and their application in tissue engineering. *Lab Chip* **12**, 45–59 (2012).
51. Hsiao, A. Y. et al. Microfluidic system for formation of PC-3 prostate cancer co-culture spheroids. *Biomaterials* **30**, 3020–3027 (2009).
52. Liu, K., Ding, H.-J., Liu, J., Chen, Y. & Zhao, X.-Z. Shape-controlled production of biodegradable calcium alginate gel microparticles using a novel microfluidic device. *Langmuir* **22**, 9453–9457 (2006).
53. Liu, Z. et al. Shape-controlled high cell-density microcapsules by electrodeposition. *Acta Biomater.* **37**, 93–100 (2016).
54. Liu, Z. et al. Three-dimensional hepatic lobule-like tissue constructs using cell-microcapsule technology. *Acta Biomater.* **50**, 178–187 (2017).
55. Liu, Z. et al. Mild formation of core-shell hydrogel microcapsules for cell encapsulation. *Biofabrication* **13**, 025002 (2021).
56. Liu, Z. et al. In vitro mimicking the morphology of hepatic lobule tissue based on Ca-alginate cell sheets. *Biomed. Mater.* **13**, 035004 (2018).

57. Wu, Z. et al. Open aerosol microfluidics enable orthogonal compartmentalized functionalization of hydrogel particles. *Matter* **7**, 3645–3657 (2024).
58. Ghiasi, Z., Sajadi, T. A. & Tafaghodi, M. Preparation and in vitro characterization of alginate microspheres encapsulated with autoclaved Leishmania major (ALM) and CpG-ODN. *Iran. J. Basic Med. Sci.* **10**, 90–98 (2007).
59. Pestovsky, Y. S. & Martínez-Antonio, A. The synthesis of alginate microparticles and nanoparticles. *Drug Des. Intell. Prop. Int. J.* **3**, 293–327 (2019).
60. Łętocha, A., Miastkowska, M. & Sikora, E. Preparation and characteristics of alginate microparticles for food, pharmaceutical and cosmetic applications. *Polymers* **14**, 3834 (2022).
61. Chaudhuri, O., Cooper-White, J., Janmey, P. A., Mooney, D. J. & Shenoy, V. B. Effects of extracellular matrix viscoelasticity on cellular behaviour. *Nature* **584**, 535–546 (2020).
62. Eliahoo, P. et al. Viscoelasticity in 3D cell culture and regenerative medicine: measurement techniques and biological relevance. *ACS Mater. Au* **4**, 354–384 (2024).
63. Shaebani, M. R. et al. Effects of vimentin on the migration, search efficiency, and mechanical resilience of dendritic cells. *Biophys. J.* **121**, 3950–3961 (2022).
64. Zohorsky, K. & Mequanint, K. Designing biomaterials to modulate notch signaling in tissue engineering and regenerative medicine. *Tissue Eng.* **27**, 383–410 (2021).
65. Kim, M. M. *Ligand-Immobilized Biomaterial Surfaces for Notch Signaling and T Cell Differentiation*. PhD thesis, University of Texas at Austin (2012).
66. Frank, V. et al. Frequent mechanical stress suppresses proliferation of mesenchymal stem cells from human bone marrow without loss of multipotency. *Sci. Rep.* **6**, 24264 (2016).
67. Dingal, P. D. P. & Discher, D. E. Combining insoluble and soluble factors to steer stem cell fate. *Nat. Mater.* **13**, 532–537 (2014).
68. Fernandes, R. A. et al. A cell topography-based mechanism for ligand discrimination by the T cell receptor. *Proc. Natl Acad. Sci. USA* **116**, 14002–14010 (2019).
69. Voisinne, G. et al. Kinetic proofreading through the multi-step activation of the ZAP70 kinase underlies early T cell ligand discrimination. *Nat. Immunol.* **23**, 1355–1364 (2022).
70. Feng, Y., Reinherz, E. L. & Lang, M. J.  $\alpha\beta$  T cell receptor mechanosensing forces out serial engagement. *Trends Immunol.* **39**, 596–609 (2018).
71. Liu, B., Chen, W., Evavold, B. D. & Zhu, C. Accumulation of dynamic catch bonds between TCR and agonist peptide-MHC triggers T cell signaling. *Cell* **157**, 357–368 (2014).
72. Saitakis, M. et al. Different TCR-induced T lymphocyte responses are potentiated by stiffness with variable sensitivity. *eLife* **6**, e23190 (2017).
73. Ma, Z., Janmey, P. A. & Finkel, T. H. The receptor deformation model of TCR triggering. *FASEB J.* **22**, 1002–1008 (2008).
74. Sunshine, J. C., Perica, K., Schneck, J. P. & Green, J. J. Particle shape dependence of CD8<sup>T</sup> T cell activation by artificial antigen presenting cells. *Biomaterials* **35**, 269–277 (2014).
75. Harding, F. A., McArthur, J. G., Gross, J. A., Rautel, D. H. & Allison, J. P. CD28-mediated signalling co-stimulates murine T cells and prevents induction of anergy in T-cell clones. *Nature* **356**, 607–609 (1992).
76. Martinsen, A., Skjak-Braek, G. & Smidsrod, O. Alginate as immobilization material: I. Correlation between chemical and physical properties of alginate gel beads. *Biotechnol. Bioeng.* **33**, 79–89 (1989).
77. Fan, Y. et al. Alginate enhances memory properties of antitumor CD8<sup>T</sup> T cells by promoting cellular antioxidation. *ACS Biomater. Sci. Eng.* **5**, 4717–4725 (2019).
78. Charbonier, F., Indiana, D. & Chaudhuri, O. Tuning viscoelasticity in alginate hydrogels for 3D cell culture studies. *Curr. Protoc.* **1**, e124 (2021).
79. Majedi, F. S. et al. Systemic enhancement of antitumor immunity by peritumorally implanted immunomodulatory macroporous scaffolds. *Nat. Biomed. Eng.* **7**, 56–71 (2023).
80. Li, Y.-R. et al. Generation of allogeneic CAR-NKT cells from hematopoietic stem and progenitor cells using a clinically guided culture method. *Nat. Biotechnol.* **43**, 329–344 (2024).
81. Li, Y.-R. et al. Allogeneic CD33-directed CAR-NKT cells for the treatment of bone marrow-resident myeloid malignancies. *Nat. Commun.* **16**, 1248 (2025).
82. Majedi, F. S. et al. Augmentation of T-cell activation by oscillatory forces and engineered antigen-presenting cells. *Nano Lett.* **19**, 6945–6954 (2019).
83. Chaudhuri, O. et al. Substrate stress relaxation regulates cell spreading. *Nat. Commun.* **6**, 6365 (2015).
84. Chen, J. Y. et al. Cell-sized lipid vesicles as artificial antigen-presenting cells for antigen-specific T cell activation. *Adv. Healthc. Mater.* **12**, e2203163 (2023).
85. Omotoso, M. O. et al. Alginate-based artificial antigen presenting cells expand functional CD8<sup>(+)T</sup> T cells with memory characteristics for adoptive cell therapy. *Biomaterials* **313**, 122773 (2025).
86. Olden, B. R. et al. Cell-templated silica microparticles with supported lipid bilayers as artificial antigen-presenting cells for T cell activation. *Adv. Healthc. Mater.* **8**, e1801188 (2019).
87. Lou, J. et al. Surface-functionalized microgels as artificial antigen-presenting cells to regulate expansion of T cells. *Adv. Mater.* **36**, e2309860 (2024).
88. Vasquez, J. M. et al. In situ forming hyperbranched PEG-thiolated hyaluronic acid hydrogels with honey-mimetic antibacterial properties. *Front. Bioeng. Biotechnol.* **9**, 742135 (2021).
89. Huang, X. et al. DNA scaffolds enable efficient and tunable functionalization of biomaterials for immune cell modulation. *Nat. Nanotechnol.* **16**, 214–223 (2021).
90. Hammink, R. et al. Semiflexible immunobrushes induce enhanced T cell activation and expansion. *ACS Appl. Mater. Interfaces* **13**, 16007–16018 (2021).
91. Philip, R. & Epstein, L. B. Tumour necrosis factor as immunomodulator and mediator of monocyte cytotoxicity induced by itself,  $\gamma$ -interferon and interleukin-1. *Nature* **323**, 86–89 (1986).
92. Frei, K. et al. Antigen presentation and tumor cytotoxicity by interferon- $\gamma$ -treated microglial cells. *Eur. J. Immunol.* **17**, 1271–1278 (1987).
93. Strzalka, W. & Ziemiencowicz, A. Proliferating cell nuclear antigen (PCNA): a key factor in DNA replication and cell cycle regulation. *Ann. Bot.* **107**, 1127–1140 (2011).
94. Bologna-Molina, R., Mosqueda-Taylor, A., Molina-Frechero, N., Mori-Estevez, A. D. & Sánchez-Acuña, G. Comparison of the value of PCNA and Ki-67 as markers of cell proliferation in ameloblastic tumor. *Med. Oral. Patol. Oral. Cir. Bucal* **18**, e174 (2012).
95. Blank, C. U. et al. Defining 'T cell exhaustion'. *Nat. Rev. Immunol.* **19**, 665–674 (2019).
96. Zhong, M. et al. BET bromodomain inhibition rescues PD-1-mediated T-cell exhaustion in acute myeloid leukemia. *Cell Death Dis.* **13**, 671 (2022).
97. Mueller, G. & Lipp, M. Shaping up adaptive immunity: the impact of CCR7 and CXCR5 on lymphocyte trafficking. *Microcirculation* **10**, 325–334 (2003).
98. Gattinoni, L., Klebanoff, C. A. & Restifo, N. P. Paths to stemness: building the ultimate antitumor T cell. *Nat. Rev. Cancer* **12**, 671–684 (2012).
99. Gattinoni, L. et al. Wnt signaling arrests effector T cell differentiation and generates CD8<sup>T</sup> memory stem cells. *Nat. Med.* **15**, 808–813 (2009).
100. Tiberti, S. et al. GZMK<sup>high</sup> CD8<sup>T</sup> T effector memory cells are associated with CD15<sup>high</sup> neutrophil abundance in non-metastatic colorectal tumors and predict poor clinical outcome. *Nat. Commun.* **13**, 6752 (2022).
101. Gounari, F. & Khazaie, K. TCF-1: a maverick in T cell development and function. *Nat. Immunol.* **23**, 671–678 (2022).

## Acknowledgements

We extend our gratitude to the UCLA Division of Laboratory Animal Medicine (DLAM) for assistance with animal studies, the UCLA BSCRC Flow Cytometry Core Facility for cell sorting, and the UCLA TCGB for scRNA-seq services. The UCLA CFAR Virology Core is acknowledged for providing human PBMCs, and the Advanced Light Microscopy/Spectroscopy Laboratory along with the Leica Microsystems Center at the California NanoSystems Institute (CNSI) for support with imaging. Additionally, we thank the NIH Tetramer Facility for providing tetramers utilized in this research. L.Y. is a member of UCLA Parker Institute for Cancer Immunotherapy (PIC). Y.-R.L. is supported by a UCLA Chancellor's Award for Postdoctoral Research and a UCLA Goodman-Luskin Microbiome Center Collaborative Research Fellowship.

## Author contributions

Z. Liu, Y.-R.L. and Y. Yang developed and optimized the protocol. Z. Liu, Y.-R.L., Y. Yang, E.Z., H.N., Y. Yan, B.Z., G.C., N.P. and Z.L. performed the protocol validation and optimization experiments. Z. Liu, Y.-R.L., Y. Yang and E.Z. analyzed and compiled the data. Z. Liu, Y.-R.L., Y. Yang, E.Z. and J.L. documented and prepared the protocol steps and procedures. L.Y. and S.L. supervised the protocol development and provided critical insights throughout the study. Z. Liu, Y.-R.L., Y. Yang, L.Y. and S.L. wrote and revised the manuscript, incorporating feedback from all authors.

## Competing interests

Z. Liu, Y.-R.L., L.Y. and S.L. filed a patent application (PCT/US24/22516) on synthetic cell as inventors. The other authors declare no competing interests.

## Additional information

**Supplementary information** The online version contains supplementary material available at <https://doi.org/10.1038/s41596-025-01265-2>.

**Correspondence and requests for materials** should be addressed to Lili Yang or Song Li.

**Peer review information** *Nature Protocols* thanks Xiao Huang, Paolo Provenzano, Qinghe Zeng, and the other, anonymous, reviewer(s) for their contribution to the peer review of this work.

**Reprints and permissions information** is available at [www.nature.com/reprints](http://www.nature.com/reprints).

**Publisher's note** Springer Nature remains neutral with regard to jurisdictional claims in published maps and institutional affiliations.

Springer Nature or its licensor (e.g. a society or other partner) holds exclusive rights to this article under a publishing agreement with the author(s) or other rightsholder(s); author self-archiving of the accepted manuscript version of this article is solely governed by the terms of such publishing agreement and applicable law.

© Springer Nature Limited 2025

## Reporting Summary

Nature Portfolio wishes to improve the reproducibility of the work that we publish. This form provides structure for consistency and transparency in reporting. For further information on Nature Portfolio policies, see our [Editorial Policies](#) and the [Editorial Policy Checklist](#).

### Statistics

For all statistical analyses, confirm that the following items are present in the figure legend, table legend, main text, or Methods section.

n/a Confirmed

- The exact sample size ( $n$ ) for each experimental group/condition, given as a discrete number and unit of measurement
- A statement on whether measurements were taken from distinct samples or whether the same sample was measured repeatedly
- The statistical test(s) used AND whether they are one- or two-sided  
*Only common tests should be described solely by name; describe more complex techniques in the Methods section.*
- A description of all covariates tested
- A description of any assumptions or corrections, such as tests of normality and adjustment for multiple comparisons
- A full description of the statistical parameters including central tendency (e.g. means) or other basic estimates (e.g. regression coefficient) AND variation (e.g. standard deviation) or associated estimates of uncertainty (e.g. confidence intervals)
- For null hypothesis testing, the test statistic (e.g.  $F$ ,  $t$ ,  $r$ ) with confidence intervals, effect sizes, degrees of freedom and  $P$  value noted  
*Give  $P$  values as exact values whenever suitable.*
- For Bayesian analysis, information on the choice of priors and Markov chain Monte Carlo settings
- For hierarchical and complex designs, identification of the appropriate level for tests and full reporting of outcomes
- Estimates of effect sizes (e.g. Cohen's  $d$ , Pearson's  $r$ ), indicating how they were calculated

*Our web collection on [statistics for biologists](#) contains articles on many of the points above.*

### Software and code

Policy information about [availability of computer code](#)

Data collection

Anton Paar RheoCompass™ software (version 1.31.70): This software collects, manages, and analyzes the rheological data.

BD FACSDiva™ software (version 6.0): This flow cytometer, used to determine the average antibody density per SynVAC, is typically operated using the BD FACSDiva™ software, which collects and analyzes flow cytometry data.

ZEISS Fluorescence Microscope ZEN (blue edition, version 2.3): This software is to manage and analyze data from ZEISS microscopes.

SEM (Scanning Electron Microscope) Tecnai User Interface 4.0: The FEI Tecnai Software is used for SEM.

Data analysis

FlowJo (version 10.6.2): FlowJo is a widely-used commercial software package for analyzing flow cytometry data. We used it to process and analyze data generated from flow cytometry experiments.

GraphPad Prism (version 8.4.3): GraphPad Prism is a commercial software used for creating scientific graphs and performing statistical analyses. We used it for graph generation and statistical analyses in our study.

R (version 4.0.3): R is an open-source programming language for statistical computing and graphics. We used it for various statistical analyses and data visualization tasks in our study.

For manuscripts utilizing custom algorithms or software that are central to the research but not yet described in published literature, software must be made available to editors and reviewers. We strongly encourage code deposition in a community repository (e.g. GitHub). See the Nature Portfolio [guidelines for submitting code & software](#) for further information.

## Data

Policy information about [availability of data](#)

All manuscripts must include a [data availability statement](#). This statement should provide the following information, where applicable:

- Accession codes, unique identifiers, or web links for publicly available datasets
- A description of any restrictions on data availability
- For clinical datasets or third party data, please ensure that the statement adheres to our [policy](#)

**Data Availability.** The main data supporting the results in this study are available within the paper. All data generated in this study, including source data for the figures, are available from figshare with the identifier.

**Code Availability.**

Single-cell RNA sequencing (scRNA-seq) data generated from this study, the processed cell matrix, data tables (e.g., expression values), and metadata have been made available in the public repository Gene Expression Omnibus (GEO) database (GSE242531).

## Research involving human participants, their data, or biological material

Policy information about studies with [human participants or human data](#). See also policy information about [sex, gender \(identity/presentation\), and sexual orientation](#) and [race, ethnicity and racism](#).

### Reporting on sex and gender

*Use the terms sex (biological attribute) and gender (shaped by social and cultural circumstances) carefully in order to avoid confusing both terms. Indicate if findings apply to only one sex or gender; describe whether sex and gender were considered in study design; whether sex and/or gender was determined based on self-reporting or assigned and methods used.*

*Provide in the source data disaggregated sex and gender data, where this information has been collected, and if consent has been obtained for sharing of individual-level data; provide overall numbers in this Reporting Summary. Please state if this information has not been collected.*

*Report sex- and gender-based analyses where performed, justify reasons for lack of sex- and gender-based analysis.*

### Reporting on race, ethnicity, or other socially relevant groupings

*Please specify the socially constructed or socially relevant categorization variable(s) used in your manuscript and explain why they were used. Please note that such variables should not be used as proxies for other socially constructed/relevant variables (for example, race or ethnicity should not be used as a proxy for socioeconomic status).*

*Provide clear definitions of the relevant terms used, how they were provided (by the participants/respondents, the researchers, or third parties), and the method(s) used to classify people into the different categories (e.g. self-report, census or administrative data, social media data, etc.)*

*Please provide details about how you controlled for confounding variables in your analyses.*

### Population characteristics

*Describe the covariate-relevant population characteristics of the human research participants (e.g. age, genotypic information, past and current diagnosis and treatment categories). If you filled out the behavioural & social sciences study design questions and have nothing to add here, write "See above."*

### Recruitment

*Describe how participants were recruited. Outline any potential self-selection bias or other biases that may be present and how these are likely to impact results.*

### Ethics oversight

*Identify the organization(s) that approved the study protocol.*

Note that full information on the approval of the study protocol must also be provided in the manuscript.

## Field-specific reporting

Please select the one below that is the best fit for your research. If you are not sure, read the appropriate sections before making your selection.

- Life sciences       Behavioural & social sciences       Ecological, evolutionary & environmental sciences

For a reference copy of the document with all sections, see [nature.com/documents/nr-reporting-summary-flat.pdf](https://www.nature.com/documents/nr-reporting-summary-flat.pdf)

## Life sciences study design

All studies must disclose on these points even when the disclosure is negative.

### Sample size

Sample sizes were based on previous studies of T cell activation using artificial antigen-presenting platforms and power analyses to detect statistically significant differences in T cell expansion, CAR transduction efficiency, and tumor killing. For flow cytometry (Fig. 5c), n = 3 or n = 6 independent biological replicates were used as indicated. For in vitro cytotoxicity assays (Fig. 6c,e), n = 4 biological replicates were used. These sample sizes are sufficient to ensure reproducibility and statistical significance (P < 0.001 or P < 0.0001).

### Data exclusions

No data were excluded from the analyses unless cells failed viability gating (e.g., <70%) or flow cytometry sample acquisition was incomplete (<10,000 events). These exclusion criteria were pre-established to ensure data quality and consistency.

### Replication

All experiments were repeated multiple times under identical conditions and all data were collected and analyzed blind to avoid any potential

bias. There were no instances of findings that were not replicated or could not be reproduced in our study.

Randomization

T cells from the same donor were randomly allocated to different activation conditions (e.g., Synthetic Cells vs. Dynabeads) within the same experiment to minimize variability due to donor effects. Tumor cell lines were randomly assigned to treatment conditions in the in vitro killing assays.

Blinding

Experiments were not blinded, as the Synthetic Cell platform and Dynabeads differ in appearance and handling protocols. However, data acquisition via flow cytometry and scRNA-seq was performed in an unbiased and standardized manner. Data analysis was conducted using pre-defined gating and clustering strategies.

## Reporting for specific materials, systems and methods

We require information from authors about some types of materials, experimental systems and methods used in many studies. Here, indicate whether each material, system or method listed is relevant to your study. If you are not sure if a list item applies to your research, read the appropriate section before selecting a response.

### Materials & experimental systems

n/a	Involved in the study
<input type="checkbox"/>	<input checked="" type="checkbox"/> Antibodies
<input type="checkbox"/>	<input checked="" type="checkbox"/> Eukaryotic cell lines
<input checked="" type="checkbox"/>	<input type="checkbox"/> Palaeontology and archaeology
<input checked="" type="checkbox"/>	<input type="checkbox"/> Animals and other organisms
<input checked="" type="checkbox"/>	<input type="checkbox"/> Clinical data
<input checked="" type="checkbox"/>	<input type="checkbox"/> Dual use research of concern
<input checked="" type="checkbox"/>	<input type="checkbox"/> Plants

### Methods

n/a	Involved in the study
<input checked="" type="checkbox"/>	<input type="checkbox"/> ChIP-seq
<input type="checkbox"/>	<input checked="" type="checkbox"/> Flow cytometry
<input checked="" type="checkbox"/>	<input type="checkbox"/> MRI-based neuroimaging

## Antibodies

Antibodies used

All antibodies used in this study, including supplier name, catalog number, clone, and RRID, are listed in detail in the Reagents section of the Methods. For example: Anti-human CD3 (Clone OKT3, BioLegend Cat# 317302, RRID: AB\_571927) Anti-human CD8 (Clone SK1, BD Cat# 348793, RRID: AB\_400383) Anti-human CD62L (Clone DREG-56, BioLegend Cat# 980706, RRID: AB\_3097278) Anti-mouse CD4 (Clone GK1.5, BioLegend Cat# 100406, RRID: AB\_312691) Anti-mouse CD95 (Clone SA367H8, BioLegend Cat# 152610, RRID: AB\_2632905)

Validation

All antibodies used are commercially available and validated by the manufacturers for flow cytometry in human or mouse samples. Validation information is available on supplier websites (e.g., BioLegend, BD Biosciences, Thermo Fisher), including datasheets with flow cytometry staining on PBMCs or known positive/negative cell lines. Where applicable, antibodies were used at recommended dilutions, and appropriate isotype and unstained controls were included to ensure specificity.

## Eukaryotic cell lines

Policy information about [cell lines and Sex and Gender in Research](#)

Cell line source(s)

All human tumor cell lines (Raji, NALM6, OVCAR3, OVCAR8, ASPC1, H226, HCC1806) were obtained from ATCC. These are well-established immortalized lines and do not have donor sex information specified. Primary mouse T cells were isolated from the spleen of C57BL/6 mice using a pan T cell isolation kit, with CD3+ T cells procured for polyclonal activation studies. Healthy donors human PBMCs were sourced from the UCLA/CFAR Virology Core Laboratory, in compliance with federal and state regulations, with no identifying information provided.

Authentication

All cell lines were obtained directly from ATCC, which performs routine authentication. Cell lines were maintained for fewer than 20 passages and were not re-authenticated during the study. Primary mouse T cells were authenticated by confirming specific surface markers, such as CD3. Human PBMCs, sourced from the UCLA/CFAR Virology Core Laboratory, were authenticated by checking for specific surface markers.

Mycoplasma contamination

All cell lines were routinely tested for mycoplasma contamination using PCR-based detection and confirmed to be negative prior to experimental use.

Commonly misidentified lines (See [ICLAC](#) register)

None of the cell lines used in this study are listed as commonly misidentified in the ICLAC database.

## Plants

Seed stocks	Report on the source of all seed stocks or other plant material used. If applicable, state the seed stock centre and catalogue number. If plant specimens were collected from the field, describe the collection location, date and sampling procedures.
Novel plant genotypes	Describe the methods by which all novel plant genotypes were produced. This includes those generated by transgenic approaches, gene editing, chemical/radiation-based mutagenesis and hybridization. For transgenic lines, describe the transformation method, the number of independent lines analyzed and the generation upon which experiments were performed. For gene-edited lines, describe the editor used, the endogenous sequence targeted for editing, the targeting guide RNA sequence (if applicable) and how the editor was applied.
Authentication	Describe any authentication procedures for each seed stock used or novel genotype generated. Describe any experiments used to assess the effect of a mutation and, where applicable, how potential secondary effects (e.g. second site T-DNA insertions, mosaicism, off-target gene editing) were examined.

## Flow Cytometry

### Plots

Confirm that:

- The axis labels state the marker and fluorochrome used (e.g. CD4-FITC).
- The axis scales are clearly visible. Include numbers along axes only for bottom left plot of group (a 'group' is an analysis of identical markers).
- All plots are contour plots with outliers or pseudocolor plots.
- A numerical value for number of cells or percentage (with statistics) is provided.

### Methodology

Sample preparation	Human PBMCs were isolated from healthy donors and cryopreserved until use. T cells were activated using Synthetic Cells or Dynabeads and expanded over 10–14 days. For flow cytometry analysis, cells were harvested, washed in PBS + 1% FBS, and stained with fluorochrome-conjugated antibodies targeting CD3, CD4, CD8, CD45RO, CD69, CD62L, TCF7, LEF1, and other markers according to manufacturer's instructions. Dead cells were excluded using Fixable Viability Dye eFluor™ 506.
Instrument	The instrument used for data collection in these experiments is the flow cytometer LSRII, produced by BD Biosciences.
Software	The software used to analyze the flow cytometry data in these experiments was FlowJo v10.
Cell population abundance	Cell sorting was not performed as part of the experiments.
Gating strategy	<p>The gating strategy used in flow cytometry typically commences with a Forward Scatter (FSC) versus Side Scatter (SSC) plot, which helps discriminate cells based on size (FSC) and internal complexity or granularity (SSC). An initial gate, generally polygonal or elliptical, is drawn around the main population of interest to exclude debris, dead cells, or doublets.</p> <p>Subsequently, this gated population is further assessed for specific marker expressions. In this study, the gating strategy might have involved gating on the CD3+ population (T cells) within the initial FSC/SSC gate. Further gates might have been applied on CD8+ T cells, and subsequent analysis of the expression of markers such as CCR7, CD45RA, and CD95 within this population could have been performed. The gating strategy is provided in the supporting material.</p>

- Tick this box to confirm that a figure exemplifying the gating strategy is provided in the Supplementary Information.